In-medium effects in ϕ meson production in heavy-ion collisions from subthreshold to relativistic energies

Taesoo Song [1,*] Joerg Aichelin,[2,3,†] and Elena Bratkovskaya[1,4,5,‡]

[1]*GSI Helmholtzzentrum für Schwerionenforschung GmbH, Planckstrasse 1, 64291 Darmstadt, Germany*
[2]*SUBATECH UMR 6457 (IMT Atlantique, Université de Nantes, IN2P3/CNRS), 4 Rue Alfred Kastler, F-44307 Nantes, France*
[3]*Frankfurt Institute for Advanced Studies, Ruth-Moufang-Strasse 1, 60438 Frankfurt am Main, Germany*
[4]*Institute for Theoretical Physics, Johann Wolfgang Goethe Universität, Frankfurt am Main, Germany*
[5]*Helmholtz Research Academy Hesse for FAIR (HFHF), GSI Helmholtz Center for Heavy Ion Physics,
Campus Frankfurt, 60438 Frankfurt, Germany*

We investigate the hidden strange ϕ meson production in heavy-ion collisions from subthreshold ($E_{\rm kin} \approx 1A$ GeV) to relativistic ($E_{\rm kin} \approx 21A$ TeV) energies as well as its coupling to the open strange mesons (kaons, antikaons) and their productions. Our study is based on the off-shell microscopic parton-hadron-string dynamics (PHSD) transport approach which is applicable for the dynamical description of strongly interacting hadronic and partonic degrees-of-freedom created in heavy-ion collisions. Implementing novel meson-baryon and meson-hyperon production channels for ϕ mesons, calculated within a T-matrix coupled-channel approach based on the extended SU(6) chiral effective Lagrangian model, along with the collisional broadening of the ϕ-meson in-medium spectral function, we find a substantial enhancement of ϕ meson production in heavy-ion collisions, especially at sub- and near-thresholds. This allows us to describe the experimentally observed strong enhancement of the ϕ/K^- ratio at low energies without including hypothetical decays of heavy baryonic resonances to ϕ as in alternative approaches. Moreover, we show that in spite of a stronger contribution from enhanced ϕ to K^- production, the majority of the experimental data for different $A + A$ systems at low energies favor the scenario with in-medium modifications of the kaon and antikaon properties in the hot and dense environment. Moreover, we study the influence of the final-state interactions of K, $\bar{K}$ mesons on the reconstruction of ϕ's by the invariant-mass method.

I. INTRODUCTION

The understanding of strangeness production in heavy-ion collisions since a few decades is one of the challenging topics in heavy-ion physics. Strangeness is a newly produced flavor, since initially the colliding nuclei are composed of "up" and "down" quarks only. Due to strangeness neutrality of the initial system, s and $\bar{s}$ quarks must be produced in pairs and end up in (anti-)strange mesons and baryons or are combined in mesons with "hidden" strangeness, such as the ϕ meson.

An enhancement of strangeness production in $A + A$ compared with $p + p$ collisions has been observed experimentally from low (below $E_{\rm kin} = 1A$ GeV) to ultrarelativistic ($\sqrt{s} > 100A$ GeV) energies. The reason for that is rather different at different energies. In low-energy $A + A$ collisions strangeness can be produced well below the physical threshold for $p + p$ scattering. The observed yield is much higher than expected from the enhances due to Fermi motion of the nucleons inside a nucleus. This indicates an additional mechanisms for strangeness production in heavy-ion collisions compared

with elementary reactions [1,2]. A detailed analysis, based on microscopic transport approaches, shows that one of the reasons is multistep reactions, which are absent in elementary collisions [1,3–5]. Indeed, in a primary collision two nucleons produce a baryonic resonance, e.g., a Δ resonance, which subsequently collides with another nucleon. Since a Δ is heavier than a nucleon, a ΔN collision can easier reach a sufficient $\sqrt{s}$ to produce strange hadrons than a NN collision. Moreover, the newly produced mesons, dominantly pions, contribute to strangeness production. This increases further the multiplicity of strange hadrons.

Another reason is the in-medium modification of hadron properties in the dense and hot medium created in heavy-ion collisions (cf. the reviews [2,6,7] and references therein). Different chiral models (staring from the early work of Kaplan and Nelson [8,9] and later continued by a variety of groups [10–16]) predict a modest enhancement of K^+ masses and a rather strong reduction of the K^- mass with increasing baryon density. Later calculations within the coupled-channel unitarized G-matrix approach, using meson-exchange potentials [17,18], predicted a more moderate in-medium change of antikaon masses (-40 to -60 MeV at density ρ_0), however, as well a visible broadening of the K^- spectral function in the medium. Such a mass reduction of antikaons leads

*T.Song@gsi.de
†Aichelin@subatech.in2p3.fr
‡E.Bratkovskaya@gsi.de

024903-1

to a lowering of the production threshold for antikaons in the medium and, consequently, makes the subthreshold K^- production (even forbidden kinematically in the vacuum) possible and leads to an enhancement of the K^- yield in $A + A$ collisions. On the other hand, the yield of K^+ is reduced in the medium due to the repulsive KN potential which makes kaons heavier [1,2,19]. The comparison of experimental data of the KaoS, FOPI, and HADES Collaborations for $A + A$ collisions at beam energies of $1A$–$2A$ GeV [20–27] for different observables [as multiplicities, rapidity, and p_T spectra as well as directed (v_1) and elliptic flow (v_2) with theoretical transport calculations [1–5,13,28–39]] showed the traces of in-medium modifications of the properties of (anti-)kaons as well as a sensitivity to the equation-of-state (EoS) of nuclear matter [2,36,37].

At high energies strangeness enhancement in $A + A$ versus $p + p$ collisions has been suggested as one of the signatures for the formation of a quark-gluon plasma (QGP) [40,41], since strangeness production is easier in a QGP than in a hadron gas due to the mass difference between the strange quark pair and the strange meson pair [42] or due to the larger available energy in a QGP as compared with a hadron-hadron collision in the "corona" region [43–45]. Experimentally a sharp rise and drop in the excitation function of the K^+/π^+ ratio (the so-called "horn") has been observed [46–50], predicted in Ref. [51], as an appearance of a QGP phase at a center-of-mass energy of $\sqrt{s_{NN}} \approx 7$ GeV. In Refs. [52,53] the horn phenomenon has been explained from a microscopic point employing the parton-hadron-string dynamics (PHSD) approach [54–59] as an interplay between chiral symmetry restoration (CSR) in the dense and hot hadronic medium (which modifies the Schwinger mechanism [60] for the hadronic particle production via the string formation and decay) and the formation of the QGP.

Strangeness enhancement is seen not only for "open" strange mesons and baryons, but also for hidden strange states as the ϕ meson, which contains a s and $\bar{s}$ quark. According to the Okubo-Zweig-Iizuka (OZI) rule [61–63], the ϕ meson dominantly decays to the open strange K, $\bar{K}$ pair and not to light quark mesons. Thus, the ϕ dynamics in heavy-ion collisions is directly coupled to the kaon and antikaon dynamics.

Since ϕ meson production is strongly suppressed as compared with other light vector mesons (ρ and ω), it is a very challenging task to measure ϕ's experimentally. One way is to measure the ϕ via dilepton decay $\phi \to e^+e^-$, which provides a clear signal, since dileptons are not affected by the strong interaction. However, the small branching ratio of the ϕ meson to dileptons makes this measurement very complicated. Another way is to measure the K^+K^- pairs from the ϕ meson decay. This process has a large branching ratio; however, there are other difficulties related to the final-state interaction of the decay products. K^+ and K^- scatter elastically and inelastically in the hadronic medium. Especially the K^- mesons with a low momentum have a large scattering cross section with nucleons. If the K^+, K^- scatter or are being absorbed, the ϕ cannot be reconstructed anymore by the invariant-mass method; thus, the experimentally "measured" ϕ multiplicity is less than the real number of ϕ produced in the reactions and its mass distribution is distorted by the final-state interaction.

Recently it has been reported by the HADES collaboration that ϕ mesons are also produced at relatively large quantities in Au + Au collisions at subthreshold energies and reach 1×10^{-4} at 1.23 A GeV [64]. Besides the ϕ multiplicity also the ratio of hidden strangeness to open strangeness has been measured and reaches values of ≈ 0.5 [64]. The same tendency of an enhanced ϕ production in Ni + Ni and Al + Al collisions at 1.93 A GeV has been reported earlier by the FOPI Collaboration [65,66]. With increasing beam energy the ratio decreases to 0.2 as has been measured recently by the STAR Collaboration [67] and becomes relatively small (≈ 0.15) already at $\sqrt{s_{NN}} \approx 4$ GeV; at high energies the dependence on the collision energy is mild [46–50].

One of the early theoretical attempts to explain these FOPI data was presented in Ref. [68] where in the RVUU transport model ϕ production by scattering of Δ resonances with nucleons and pions as well as $\Delta\Delta$ scattering were included. The BB, mB cross sections were defined within a chiral Lagrangian model. These studies came to the conclusion that these processes cannot fully account for the measured ϕ yield. Similar conclusions have been found in other transport calculations [69].

The experimentally observed high ϕ multiplicity and the surprising behavior of the ϕ/K^- ratio have triggered theoretical activities since both are higher than predicted by transport approaches. Both—along with the ϕ/Ξ^- ratio—can find an explanation if one assumes that high-lying nuclear resonances (N^* with masses above 2 GeV) have a considerable branching ratio into ϕ through $N^* \to N + \phi$. Such a scenario has been proposed in a UrQMD study [70] by accounting for $N^*(1990)$, $N^*(2080)$, $N^*(2190)$, $N^*(2220)$, and $N^*(2250)$ states decaying to ϕ mesons with a branching ratio $\approx 0.2\%$. According to [70] the formation of such heavy states in $A + A$ collisions is enhanced due to Fermi motion and secondary meson-baryon collisions while their excitation in $p + p$ collisions is small and does not contribute significantly to the near threshold data of ϕ production measured by the ANKE Collaboration [71]. This idea has been taken over later by the SMASH group in Ref. [72], applying, however, a much larger branching ratio of 0.5%. The possibility of N^* decay to other vector mesons—ω—has been discussed in Ref. [73]. The decay of heavy baryonic resonances to ϕ mesons, however, has not been observed experimentally so far [74].

The goal of this study is to show that the observed "enhanced" ϕ multiplicity and ϕ/K^- ratio close to threshold can be understood also in a more conventional approach:

(i) By incorporating the dynamical modifications of the ϕ meson properties in the medium such as a collisional broadening of the ϕ meson spectral function.

(ii) By accounting for additional multistep meson-baryon and meson-hyperon reactions for ϕ meson production as predicted by the SU(6) extension of the meson-baryon chiral Lagrangian within a unitary coupled-channel T-matrix approach. These reactions of produced mesons and/or baryonic nonstrange strange resonance become possible in heavy-ion collision and lead to an enhancement of the ϕ yield.

As a theoretical laboratory for our study we use the microscopic PHSD transport approach [54,58,59] which is based on Kadanoff-Baym off-shell dynamics suited for the description of strongly interacting hadronic and partonic systems. The PHSD has been intensively applied for studying the in-medium effects and strangeness production in $p + A$ and $A + A$ collisions from low to ultrarelativistic energies [35,53,58,59,75].

The consequences of the partial chiral symmetry restoration of the ϕ meson properties in a hot and/or dense matter are expected to be seen in proton-nucleus and heavy-ion collisions. In the QCD sum-rule approach, the decrease of the quark condensate leads to a mass shift of the vector meson [76,77]. Theoretical calculations based on chiral models predict a mass shift as well and a broadening of the ϕ meson spectral function [78–82]. There have been many efforts to measure experimentally the in-medium properties of vector mesons in $p + A$ and $A + A$ collisions, in particular by the dilepton decay channel, as well as to describe the data in theoretical approaches (cf. the reviews [7,58]). These studies are, however, mostly concentrated on ρ or ω mesons. The very low production rate and the rather small width make it difficult to study the ϕ in-medium modification. Recently experimental evidence for observation of the in-medium effects of ϕ mesons in $p + A$ reactions has been reported by the KEK-PS E325 Collaboration [83] by measuring the dilepton spectra. On the other hand, the possibilities to observe the in-medium modification of ϕ spectral function—using the strong decay mode $\phi \rightarrow K^+ K^-$—may be also explored [84].

In this study we argue that the in-medium modification of the ϕ spectral function by collisional broadening during the propagation in the medium as well as the modification of the production cross sections in the medium play an important role for ϕ meson production as well as for the final reconstruction via the $K\bar{K}$ mode (similar to the K^* reconstruction [85]).

Further on, we argue that multistep meson-baryon reactions with newly produced mesons and baryonic resonances lead to an enhancement of ϕ production in heavy-ion collisions compared with $p + p$ reactions where such processes are not possible. In this study we substantially extend the traditionally considered $m + B$ channels involving pions, nucleons, and Δ's by accounting for s-wave scattering $m + B \rightarrow \phi + B$ reactions with $m = \eta, K, \rho, K^*$ mesons and $B = N, \Delta, \Lambda, \Sigma, \Sigma^*$ baryons for all possible $I = 1/2$ and $3/2$ channels. Since those cross sections are not known experimentally, we use T-matrix calculations based on the SU(6) extension of the meson-baryon chiral Lagrangian within a unitary coupled-channel approach [86]. We note that the in-medium effects on vector and pseudoscalar strange mesons are included via the spectral functions also for these novel channels. The backward reactions are accounted for via detailed balance.

This paper is organized as follows: in Sec. II we describe the modification of ϕ meson spectral function in the medium; in Sec. III we recall how the off-shell particle propagates in a nuclear medium. Then the ϕ meson production through elementary reactions in the nuclear medium is presented based on the coupled-channel T-matrix approach in Sec. IV, followed by the (anti)kaon production in Sec. V. Section VI is devoted

to ϕ production in heavy-ion collisions and the results are compared with experimental data. The contribution from ϕ meson decay to the (anti-)kaon yield is investigated in Sec. VII and the strange particle ratios are presented in Sec. VIII. Finally, a summary is given in Sec. IX.

II. IN-MEDIUM MODIFICATION OF ϕ MESON PROPERTIES

To explore the influence of in-medium effects on the vector-meson spectral function we introduce collisional broadening, Γ_{coll}, following the approach of Refs. [87–90]:

$$\Gamma_V^*(M, |\vec{p}|, \rho) = \Gamma_V(M) + \Gamma_{\text{coll}}(M, |\vec{p}|, \rho), \quad (1)$$

where M is the mass and $\Gamma_V(M)$ the total width of the vacuum spectral function of the vector meson ($V = \rho, \omega, \phi$). For the vacuum width of the ϕ meson we use

$$\Gamma_\phi(M) \simeq \Gamma_{\phi \rightharpoonup \rho\pi(3\pi)}^{\text{expt.}} \frac{\Gamma_{\phi \rightharpoonup \rho\pi(3\pi)}(M)}{\Gamma_{\phi \rightharpoonup \rho\pi(3\pi)}(M_0)}$$

$$+ \Gamma_{\phi \rightharpoonup K\bar{K}}^{\text{expt.}} \left(\frac{M_0}{M}\right)^2 \left(\frac{q}{q_0}\right)^3 \theta(M - 2m_K), \quad (2)$$

where M_0 is the vacuum pole mass of the vector meson spectral function and $\Gamma_i^{\text{expt.}}$ is the experimental decay width of channel i. The momentum of a ϕ meson with masses M and M_0 is given by

$$q = \frac{(M^2 - 4m_K^2)^{1/2}}{2}, \quad q_0 = \frac{(M_0^2 - 4m_K^2)^{1/2}}{2}.$$

Here $\Gamma_{\phi \rightharpoonup \rho\pi(3\pi)}(M)$ is the decay width of $\phi \rightarrow \rho\pi(3\pi)$, calculated in the effective chiral Lagrangian with parity-anomalous terms [91]. The collisional width in Eq. (1) is approximated as

$$\Gamma_{\text{coll}}(M, |\vec{p}|, \rho) = \gamma \rho < v \, \sigma_{VN}^{\text{tot}} > \approx \alpha_{\text{coll}} \frac{\rho}{\rho_0}, \quad (3)$$

where $v = |\vec{p}|/E$ is the velocity with $\vec{p}$ and E being respectively the three-momentum and energy of the vector meson in the rest frame of the nucleon current, and $\gamma^2 = 1/(1 - v^2)$. Furthermore, ρ is the nuclear density, $\rho_0 = 0.168$ fm^{-3} is the normal nuclear density, and σ_{VN}^{tot} is the meson-nucleon total cross section in vacuum. To simplify the calculations of $\Gamma_{\text{coll}}(\rho)$ we use the linear density approximation for the collisional width with coefficient α_{coll} [90]. Experimental and theoretical results constraint α_{coll} for ϕ mesons: The first is the KEK E325 experiment, where the ϕ width has been measured to be 15.3 MeV at normal nuclear matter density [83]. The second are calculations based on hadronic models, which tend to get a larger broadening (up to 40 MeV width) [81,82,92]. The value of 25 MeV, which we use in this study, is roughly the average value.

We note that the CBELSA-TAPS Collaboration has shown (for the ω meson) that the pole mass of vector mesons changes at finite baryon density [93]. We model this change following the Hatsuda-Lee [77] or Brown-Rho scaling [76] as

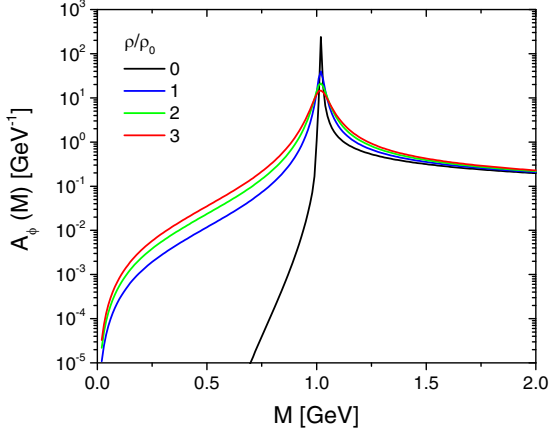$$M_0^*(\rho) = \frac{M_0}{(1 + \alpha \rho / \rho_0)}, \quad (4)$$

FIG. 1. The spectral functions of ϕ mesons in the collisional broadening scenario for nuclear densities of $0\rho_0$, $1\rho_0$, $2\rho_0$, $3\rho_0$.

where ρ is the nuclear density at the ϕ location point. $\alpha \simeq 0.12$ for the ω meson [94], and $\alpha \simeq 0.035$ for the ϕ meson. We note that the parametrization of Eq. (4) may also be employed at much higher collision energies without the need to introduce a cutoff density in order to avoid negative pole masses. Equation (4) is uniquely fixed by the standard expression $M_0^*(\rho) \approx M_0(1 - \alpha\rho/\rho_0)$ in the low-density regime. In this study, however, we consider only the broadening of the width of the ϕ mesons, neglecting the (small) mass shift in the medium.

For the spectral function of a vector meson of mass M at baryon density ρ we take a Breit-Wigner form:

$$A_V(M, \rho) = C_1 \frac{2}{\pi} \frac{M^2 \Gamma_V^*(M, \rho)}{\left[M^2 - M_0^{*2}(\rho)\right]^2 + [M\Gamma_V^*(M, \rho)]^2}, \quad (5)$$

where C_1 is fixed by the normalization condition for arbitrary ρ:

$$\int_{M_{\min}}^{M_{\lim}} A_V(M, \rho) dM = 1, \quad (6)$$

with $M_{\lim} = 2$ GeV being chosen as an upper limit for the numerical integration. The lower limit for the vacuum spectral function is given by the two-pion decay, $M_{\min} = 2m_\pi$ for a ρ meson and the three-pion decay, $M_{\min} = 3m_\pi$ for a ϕ meson decay, whereas for the in-medium collisional broadening case by $M_{\min} = 2m_e \to 0$ with m_e denoting the electron mass. M_0^* is the pole mass of the vector-meson spectral function with $M_0^*(\rho = 0) = M_0$ in vacuum. It may be shifted in the medium for the dropping mass scenario according to Eq. (4), which is, however, not considered here for ϕ mesons.

The resulting spectral function of ϕ mesons is displayed in Fig. 1 for the case of the "collisional broadening" scenario for densities of 0, 1, 2, and 3 times ρ_0. Note that the hadronic width of ϕ mesons vanishes below the three-pion mass in vacuum. With increasing nuclear density the elastic and inelastic interactions of the vector mesons shift strength towards low invariant masses.

III. OFF-SHELL PARTON-HADRON-STRING DYNAMICS APPROACH

The parton-hadron-string dynamics (PHSD) [54–59] is a microscopic covariant transport approach for the dynamical description of strongly interacting hadronic and partonic matter created in heavy-ion collisions. It is based on a solution of the Cassing-Juchem generalized off-shell transport equations for test particles [95,96] derived from the first-order gradient expansion of Kadanoff-Baym equations [97], see Refs. [55,98]. PHSD differs from the semiclassical Boltzmann-Uehing-Uhlenbeck (BUU) model, since it propagates Green's functions (in phase-space representation) which contain information not only on the occupation probability (in terms of the phase-space distribution functions), but also on the properties of hadronic and partonic degrees of freedom via their spectral functions. The PHSD approach allows us to describe the full evolution of a relativistic heavy-ion collision from the initial hard nucleon-nucleon scatterings with string formation and decay to the formation of the strongly interacting quark-gluon plasma (QGP) as well as hadronization and the subsequent interactions in the expanding hadronic phase extending the early realization of the hadron-string-dynamics (HSD) transport approach [1] by including the in-medium effects such as a collisional broadening of the vector-meson spectral functions [90] and the modification of strange degrees of freedom in line with G-matrix calculations [35,75]. Moreover, the implementation of detailed balance on the level of $2 \leftrightarrow 3$ reactions is realized for the main channels of strangeness production and absorption by baryons ($B = N, \Delta, Y$) and pions [75], as well as for the multimeson fusion reactions $2 \leftrightarrow n$ for the formation of $B + \bar{B}$ pairs [99,100].

Since the spectral function of the vector mesons (i.e., real and imaginary part of their self-energies) changes with density by collisional broadening, their propagation through the hot and dense medium can only be treated in off-shell transport approaches in a consistent way (see example in Fig. 3 of Ref. [90]).

Here we briefly describe the implementation of the off-shell transport dynamics (OSTD) in the PHSD approach (for the details of off-shell transport theory we refer the reader to the book [101]). A vector meson V—created at some space-time point x at density ρ—is distributed in mass according to its spectral function $A_V(M, \rho)$ (in the kinematically allowed region which is not excluded by energy and momentum conservation). While propagating through the nuclear medium, the self-energy and total width of the vector meson, $\Gamma_V^*(M, \rho)$ [Eq. (1)], changes dynamically. This modifies the spectral function, Eq. (5), depending on the real part of the vector-meson self-energy, $\text{Re}\Sigma^{\text{ret}}$, as well as on the imaginary part ($\Gamma_V^* \simeq -\text{Im}\Sigma^{\text{ret}}/M$):

$$A_V(M, \rho) = C_1 \frac{2}{\pi} \frac{M^2 \Gamma_V^*}{\left(M^2 - M_0^2 - \text{Re}\Sigma^{\text{ret}}\right)^2 + (M\Gamma_V^*)^2}, \quad (7)$$

which is the in-medium form for a boson spectral function. The spectral function merges to the vacuum spectral function when the ϕ leaves the medium.

In the OSTD, the general off-shell Cassing-Juchem equations of motion for test particles with three-momentum $\vec{P}_i$ and energy ε_i at position $\vec{X}_i$ read [95,96]

$$\frac{d\vec{X}_i}{dt} = \frac{1}{1 - C_{(i)}} \frac{1}{2\varepsilon_i} \left[2\vec{P}_i + \vec{\nabla}_{P_i} \mathrm{Re}\Sigma_{(i)}^{\mathrm{ret}} + \frac{\varepsilon_i^2 - \vec{P}_i^2 - M_0^2 - \mathrm{Re}\Sigma_{(i)}^{\mathrm{ret}}}{\tilde{\Gamma}_{(i)}} \vec{\nabla}_{P_i}\tilde{\Gamma}_{(i)} \right], \tag{8}$$

$$\frac{d\vec{P}_i}{dt} = -\frac{1}{1 - C_{(i)}} \frac{1}{2\varepsilon_i} \left[\vec{\nabla}_{X_i} \mathrm{Re}\Sigma_i^{\mathrm{ret}} + \frac{\varepsilon_i^2 - \vec{P}_i^2 - M_0^2 - \mathrm{Re}\Sigma_{(i)}^{\mathrm{ret}}}{\tilde{\Gamma}_{(i)}} \vec{\nabla}_{X_i}\tilde{\Gamma}_{(i)} \right], \tag{9}$$

$$\frac{d\varepsilon_i}{dt} = \frac{1}{1 - C_{(i)}} \frac{1}{2\varepsilon_i} \left[\frac{\partial \mathrm{Re}\Sigma_{(i)}^{\mathrm{ret}}}{\partial t} + \frac{\varepsilon_i^2 - \vec{P}_i^2 - M_0^2 - \mathrm{Re}\Sigma_{(i)}^{\mathrm{ret}}}{\tilde{\Gamma}_{(i)}} \frac{\partial\tilde{\Gamma}_{(i)}}{\partial t} \right], \tag{10}$$

where the notation $F_{(i)}$ implies that the function is taken at the coordinates of the test particle, i.e., $F_{(i)} \equiv F(t, \vec{X}_i(t), \vec{P}_i(t), \varepsilon_i(t))$. In Eqs. (8)–(10), $\mathrm{Re}\Sigma^{\mathrm{ret}}$ is a shorthand notation of the real part of the retarded self-energy while $\tilde{\Gamma} = -\mathrm{Im}\Sigma^{\mathrm{ret}}$ stands for the (negative) imaginary part. Apart from the propagation in the real potential $\approx \mathrm{Re}\Sigma^{\mathrm{ret}}/2\varepsilon$ the equations (8)–(10) include the dynamical changes due to the imaginary part of the self-energy $\mathrm{Im}\Sigma^{\mathrm{ret}} \approx -M\Gamma_V^*$ with Γ_V^* from Eq. (1).

In the above equations a common factor $(1 - C_{(i)})^{-1}$ appears, which includes the energy derivatives of the retarded self-energy,

$$C_{(i)} = \frac{1}{2\varepsilon_i} \left[\frac{\partial \mathrm{Re}\Sigma_{(i)}^{\mathrm{ret}}}{\partial \epsilon_i} + \frac{\varepsilon_i^2 - \vec{P}_i^2 - M_0^2 - \mathrm{Re}\Sigma_{(i)}^{\mathrm{ret}}}{\tilde{\Gamma}_{(i)}} \frac{\partial\tilde{\Gamma}_{(i)}}{\partial \epsilon_i} \right]. \tag{11}$$

This common factor leads to a rescaling of the "eigentime" of particle i but does not change the trajectories as demonstrated in Fig. 3 of Ref. [96]. According to the model studies in Ref. [96] this prefactor is negative for invariant masses M below the pole mass M_0 and positive above. This implies that the factor $1/(1 - C_i)$ is less than 1 for $M < M_0$ and larger than 1 for $M > M_0$ (as stated in Ref. [96]). This yields a time dilatation for masses $M < M_0$ in their phase-space propagation.

The interpretation of Eqs. (8)–(10) becomes particularly transparent if $\tilde{\Gamma}$ is independent on the three-momentum $\vec{P}$. Then, using $M^2 = P^2 - \mathrm{Re}\Sigma^{\mathrm{ret}}$ as an independent variable instead of the energy $P_0 \equiv \varepsilon$, Eq. (10) turns to

$$\frac{dM_i^2}{dt} = \frac{M_i^2 - M_0^2}{\tilde{\Gamma}_{(i)}} \frac{d\tilde{\Gamma}_{(i)}}{dt}. \tag{12}$$

This is the equation for the time evolution of the invariant mass squared of the test-particle i [95,96]. Now the deviation from the pole mass, $\Delta M^2 = M^2 - M_0^2$, follows the equation

$$\frac{d}{dt}\Delta M^2 = \frac{\Delta M^2}{\tilde{\Gamma}} \frac{d}{dt}\tilde{\Gamma} \leftrightarrow \frac{d}{dt}\left[\ln\left(\frac{\Delta M^2}{\tilde{\Gamma}}\right) \right] = 0, \tag{13}$$

which expresses the fact that the off-shellness of the particle is proportional to the total width.

IV. ϕ MESON PRODUCTION IN ELEMENTARY REACTIONS IN THE NUCLEAR MEDIUM

A. ϕ meson production in baryon-baryon reactions

Since the vector mesons are produced in the hot and dense medium, which is created in heavy-ion collisions, their production cross section has to be also modified compared with the vacuum cross section. However, the theoretical calculation of such in-medium cross sections is not trivial and can presently not be achieved from first-principle QCD calculations. Also a variety of effective chiral models and T-matrix approaches provide only in-medium spectral functions (cf. Ref. [112]) but no cross sections. We note that the situation in the strangeness channels is more advanced in this respect and G-matrix calculations for the in-medium cross sections are available [35,113].

In the traditional on-shell approaches, in-medium mass shifts and/or width broadening of particles have been incorporated by parametrizing the vacuum cross sections as a function of the invariant energy $\sqrt{s}$ and the threshold $\sqrt{s_0}$ (cf. Refs. [1,114,115]). In-medium modifications of cross sections then in first order have been incorporated by shifting the threshold energy $(s_0^*)^{1/2} = \sqrt{s_0} + M_0^* - M_0$ due to a lack of microscopic calculations for the corresponding in-medium transition matrix elements.

To account for the in-medium effects in production cross sections, we model the vector-meson production cross sections in NN and πN reactions in the following phenomenological way:

(i) For low-energy $BB \to \phi BB$ reactions (here $B = N, \Delta$) the total cross section for NN (or BB) scattering $\sigma_{NN \to VNN}(s, \rho)$ is given by

$$\sigma_{NN \to VNN}(s, \rho) = \int_{M_{\min}}^{M_{\max}} dM \, \frac{d\sigma_{NN \to VNN}(s, M, \rho)}{dM}. \tag{14}$$

We note in advance that a similar strategy is used for modeling $\sigma_{\pi N \to VN}(s, \rho)$.

The mass differential cross sections are approximated by

$$\frac{d\sigma_{NN \to VNN}(s, M, \rho)}{dM}$$
$$= \sigma_{NN \to VNN}^0(s, M, \rho) A_V(M, \rho) \frac{1}{\int_{M_{\min}}^{M_{\lim}} A_V(M, \rho)dM}, \tag{15}$$

where $A_V(M, \rho)$ denotes the meson spectral function, Eq. (5), for a given total width Γ_V^*, Eq. (1); $M_{\max} = \sqrt{s} - 2m_N \leqslant M_{\lim}$ is the kinematically allowed maximum invariant mass of the vector meson V and m_N is the nucleon mass. In Eq. (15) $\sigma_{NN \to VNN}^0(s, M, \rho)$ is the vacuum cross section for vector mesons with mass M (see Sec. 3.4 of Ref. [1] for the explicit parametrizations). Note that the physical threshold for the ϕ production in NN reactions is defined as $\sqrt{s_{th}} = 2m_N + M_{\min}$, i.e., for the broadening scenario $\sqrt{s_{th}} \to 2m_N + 2m_e$. For the definition of $M_{\lim}$ and $M_{\min}$ see Eq. (6).

Thus, Eq. (15) is used to model the vector-meson production in NN reactions in the vacuum and in the medium. Substituting Eq. (15) into Eq. (14), we get

$$\sigma_{NN \to VNN}(s, \rho)$$
$$= \frac{\int_{M_{\min}}^{M_{\max}} A_V(M, \rho)\sigma_{NN \to VNN}^0(s, M, \rho)dM}{\int_{M_{\min}}^{M_{\lim}} A_V(M, \rho)dM}.$$

(ii) The implementation of the in-medium effects for ϕ production from BB as well as from mB and mm reactions at high energies follows the general strategy in PHSD: the treatment of energetic $BB \to X$ collisions, leading to multiparticle production, is realized in the PHSD by the excitation of the strings based on the string LUND model [116] (see Ref. [117] for the details of the treatment of elementary collisions in the PHSD within the "tuned" LUND string model.) The threshold for the string formation is fixed to $s_{\mathrm{th(string)}}^{1/2}(BB) = 2.65$ GeV in PHSD. The in-medium spectral functions for mesonic and baryonic resonances are incorporated in the PHSD "tune" of the Lund model by including their in-medium self-energy and in-medium width depending on the local baryon density and temperature [90]. It allows us to study in-medium effects such as a collisional broadening of spectral functions of vector mesons $(\rho, \omega, \phi, a_1)$ [58,90].

The total cross section for the channel $pp \to \phi X$ is displayed in Fig. 2 as a function of the invariant energy $\sqrt{s}$ and for densities of $\rho/\rho_0 = 0, 1, 2, 3$. The arrow shows the threshold for string formation ($\sqrt{s} = 2.65$ GeV). The squares show the experimental data [102,103,105] for the inclusive vector-meson production $pp \to VX$, where X stands for all final particles including two baryons and further mesons. As seen from Fig. 2, the threshold for ϕ production shifts to lower $\sqrt{s}$ with increasing baryon density ρ, which leads to the enhancement of their production in a medium compared with the vacuum (black line).

B. ϕ meson production in meson-baryon reactions

The ϕ production by mB collisions is (similar to BB reactions) split into two regimes: the low-energy binary collisions $mB \to \phi B$ and high-energy $mB \to \phi + X$, which are realized via string formation if the $\sqrt{s}$ is above the mB string threshold $s_{\mathrm{th(string)}}^{1/2}(mB) = 2.4$ GeV. The implementation of in-medium

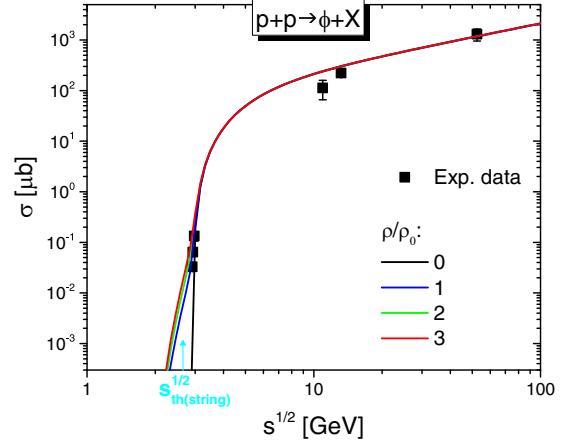
FIG. 2. Inclusive cross section for $\sigma_{pp \to \phi X}$ as a function of the invariant energy $\sqrt{s}$ calculated at $\rho/\rho_0 = 0, 1, 2, 3$, in comparison with the experimental data from Refs. [71,102–111]. The arrow indicates the threshold energy for string formation in baryon-baryon scattering.

effects is similar to the BB case discussed in the previous section. The actual parametrizations for binary $mB \to \phi B$ reactions for $m = \pi$ and $B = N, \Delta$ are taken in Breit-Wigner form—the same way as in the HSD code (see Sec. 3.5 of Ref. [1]).

In Fig. 3 we show the cross section for the $\pi N \to \phi X$ reaction versus the invariant energy $\sqrt{s}$ for baryon densities $\rho/\rho_0 = 0, 1, 2, 3$. The black line represents the $\pi N \to \phi X$ cross sections in free space while the colored lines stand for the in-medium cross sections within the collisional broadening scenario. The vertical arrow denotes the threshold for string formation in meson-baryon collisions.

As seen from Fig. 3, similar to the NN case, the πN cross section is shifted towards the low-$\sqrt{s}$ region due to the in-medium collisional broadening of the ϕ spectral function
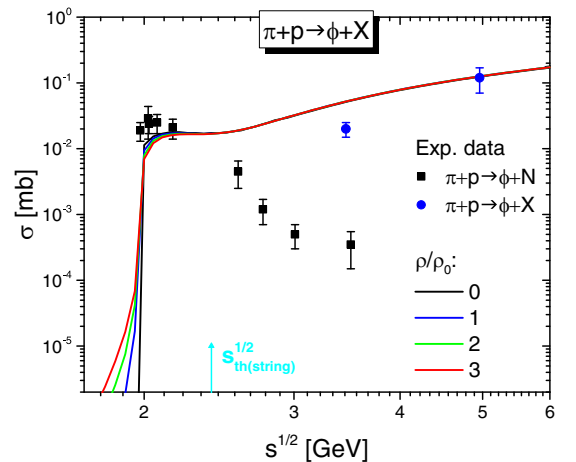

FIG. 3. Inclusive cross section for $\pi + p \to \phi + X$ as a function of the invariant energy $\sqrt{s}$ for $\rho/\rho_0 = 0, 1, 2,$ and 3 in comparison with inclusive and exclusive experimental data on ϕ production from [102,105]. The vertical arrow indicates the threshold energy for string formation in meson-baryon collisions.

which allows for ϕ production in the medium below the vacuum threshold. Consequently, the ϕ production is enhanced in heavy-ion collisions.

We note that the in-medium modifications are also accounted for the ϕ absorption and elastic-scattering cross sections. The total cross section for ϕ absorption by a nucleon $\phi + N \rightarrow X$ is parametrized by [118]

$$\sigma_{\phi N}^{\text{tot}} = 5 \text{ mb} + \frac{4.5 \text{ mb GeV}/c}{p_{\text{lab}}}, \qquad (16)$$

where p_{lab} is the ϕ meson momentum (GeV/c) in the nucleon-rest-frame.

The elastic scattering of a ϕ mesons on nucleon is taken as in Ref. [118]:

$$\sigma_{\phi N}^{\text{el}} = \frac{10 \text{ mb}}{1 + p_{\text{lab}}/(\text{GeV}/c)}. \qquad (17)$$

C. Novel $mB \rightarrow \phi B$ production channels within a SU(6) based T-matrix approach

In heavy-ion collisions even at relatively low energies, additionally to pions, nucleons, and Δ resonances, a variety of mesons and baryonic nonstrange and strange resonances are produced. Even if their abundances are small at energies of the GSI heavy-ion synchrotron (SIS), they can participate in multistep scattering which leads also to ϕ production. The AMPT transport model [119,120] includes $mB \rightarrow \phi B$ reactions with $m = \pi, \rho$, $B = N, \Delta$ as well as reactions with initial strange mesons and hyperons—$K\Lambda \rightarrow \phi N$ [121]. However, such reactions were found to be not sufficient to explain the experimental data on ϕ production at SIS energies [68]. In this study we consider additional mB channels, predicted by a meson-baryon chiral effective Lagrangian and explore their influence on ϕ production.

The consistent SU(6) extension of the meson-baryon chiral Lagrangian within a coupled-channel unitary approach allows us to include in the T-matrix a lot of other meson-baryon channels which produce a ϕ meson [86]. The s-wave scattering amplitude from the SU(6) chiral effective Lagrangian is written as

$$V_{ij}^{SIJ} = \varepsilon_{ij}^{SIJ} \frac{2\sqrt{s} - M_i - M_j}{4 f_i f_j} \sqrt{\frac{E_i + M_i}{2M_i}} \sqrt{\frac{E_j + M_j}{2M_j}}, \quad (18)$$

where i (j) indicates the initial (final) meson-baryon scattering states, $M_{i(j)}$ and $E_{i(j)}$ are, respectively, the mass and center-of-mass energy of the baryon, $f_{i(j)}$ is the decay constant of the meson to the i (j) state, and ε_{ij}^{SIJ} the degeneracy coefficient corresponding to the scattering channel with S, I, and J being total strangeness, isospin, and angular momentum of the collision, respectively [113,122].

A T-matrix approach can be formulated on the basis of the Born scattering amplitude V_{ik}^{SIJ},

$$T_{ij}^{SIJ} = V_{ij}^{SIJ} + V_{ik}^{SIJ} G_{kk}^{SIJ} T_{kj}^{SIJ}, \qquad (19)$$

where k is the intermediate meson-baryon state and the sum is performed over all possible states. G_{kk}^{SIJ} is the product of the meson and baryon propagators of the state k [123], which is

renormalized such that

$$G_{kk}^{SIJ}(s = m_N^2 + m_\pi^2) = 0, \qquad (20)$$

with m_N and m_π being nucleon and pion masses, respectively.

Since the second term of the right-hand side of Eq. (19) is factorizable in the S-wave channel, the loop momentum and $\sqrt{s}$ are separable, so the T-matrix can be expressed as

$$T_{ij}^{SIJ} = (1 - V^{SIJ} G^{SIJ})_{ik}^{-1} V_{kj}^{SIJ}, \qquad (21)$$

where $1_{jk} = \delta_{jk}$.

For ϕ production from meson-baryon S-wave scattering we explore reactions that involve amplitudes in the following sectors:

$$(I, J) = (1/2, 1/2), \ (3/2, 1/2), \ (1/2, 3/2),$$
$$(3/2, 2/2), \ (3/2, 5/2), \qquad (22)$$

and $S = 0$. The channels considered in this study for ϕ meson production are

$$\eta N, \ K\Lambda, \ K\Sigma, \ \rho N, \ K\Sigma^*, \rho\Delta, K^*\Lambda, \ K^*\Sigma, \ K^*\Sigma^* \rightarrow \phi N$$
$$(23)$$

for $I = 1/2$ and

$$K\Sigma, \ \rho N, \ \eta\Delta, \ K\Sigma^*, \ \rho\Delta, K^*\Sigma, \ K^*\Sigma^* \rightarrow \phi\Delta \quad (24)$$

for $I = 3/2$. For example, $\rho\Delta \rightarrow \phi\Delta$ has contributions from $(I, J) = (3/2, 1/2), (3/2, 3/2)$ and $(3/2, 5/2)$.

The ϕ production cross sections along with a nucleon and a Δ from the T-matrix is defined as

$$\sigma_{ij}(\sqrt{s}) = \frac{1}{4\pi} \frac{M_i M_j}{s} \frac{q_j}{q_i} \frac{\sum_J (2J+1)|T_{ij}^J|^2}{\sum_J (2J+1)}. \qquad (25)$$

Figure 4 shows the ϕ production cross sections of the mB channels for ϕN (left) and for $\phi\Delta$ (right), calculated in the T-matrix approach. All resonances here are taken with their pole mass for simplicity. One can see that the cross sections show a very strong flavor dependence. The channels with initial strange mesons and hyperons are the largest due to the OZI-rule. However, in heavy-ion collisions the relative contribution of the different mB channels is defined by the abundances of the secondary hadrons involved in the ϕ production. The η mesons are more abundant then K^*, thus their scattering with nucleons are more probable then K^* scattering with strange baryons $\Lambda, \Sigma, \Sigma^*$ even if the ηN cross section is smaller then that for K^*Y. The latter will be demonstrated in Fig. 8 in Sec. VI.

D. ϕ meson production by meson-meson reactions

Since ϕ mesons decay either into $K + \bar{K}$ or into $\rho + \pi$, they can be formed in the medium by the inverse processes: $K\bar{K} \rightarrow \phi$, $\rho + \pi \rightarrow \phi$. Additionally we take into account the low-energy channels $K + \bar{K} \rightarrow \phi + m$ and $\eta + m \rightarrow \phi + m$ with m being a meson, although their contributions are very small. We note that the ϕ production by the mm string formation is also accounted for in the PHSD, where the mm string threshold is taken as $s_{\text{th(string)}}^{1/2}(mm) = 1.3$ GeV.
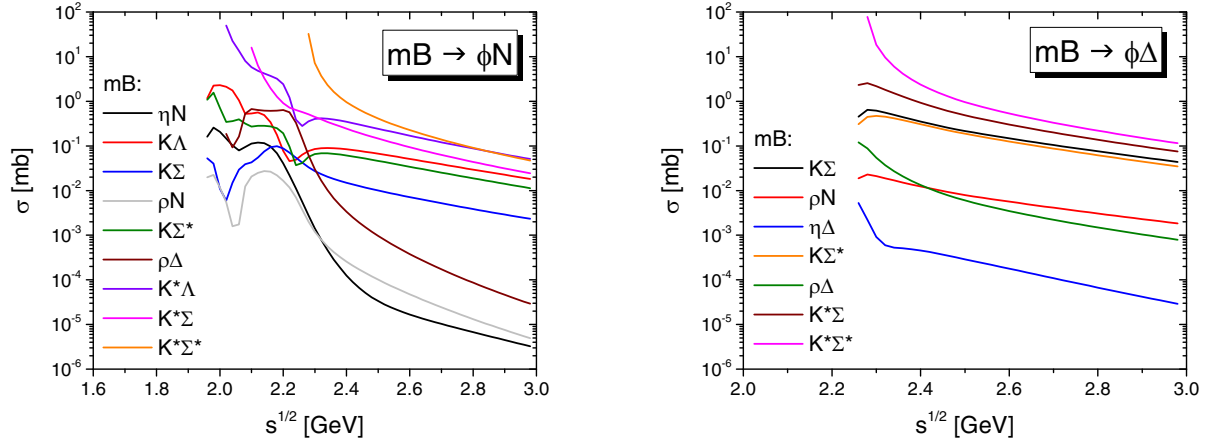
FIG. 4. Cross sections of the mB channels for ϕN production (left) and for $\phi\Delta$ production (right), calculated in the T-matrix approach. All resonances here are taken with their pole mass.

V. IN-MEDIUM STRANGENESS PRODUCTION IN THE PARTON-HADRON-STRING DYNAMICS

Before showing the PHSD results on the influence of the novel channels for ϕ meson production on the (anti-)kaon dynamics, we briefly recall the theoretical basis for including of the in-medium effects on (anti-)kaon production in heavy-ion collisions as realized in our previous work [75].

The transition amplitudes of antikaon baryon scattering as well as the self-energy of the antikaon are calculated in the G-matrix approach [113]. It is based on the self-consistent unitarization of the transition amplitude from an effective chiral Lagrangian, and the summation of the Matsubara frequencies to obtain finite-temperature results. As a result, the transition amplitudes decrease in the nuclear medium due to the Pauli blocking and the self-energy of the antikaon, which both depend on the nuclear density, the temperature, and the antikaon momentum in nuclear matter [113]. Both the real and the imaginary part of the self-energy decreases with nuclear density, while the temperature dependence is mild. Furthermore, with increasing momentum, the real part of the self-energy decreases rapidly, whereas the imaginary part of the self-energy changes only little. As a result, the spectral function of antikaons—whose pole mass is shifted by the real part of the self-energy and whose width is generated by the imaginary part of the self-energy shows a width broadening and at low momenta, $p < 300$ MeV, also a mass shift. Since both mass shift and width broadening lower the threshold energy for antikaon production, the antikaon yield in heavy-ion collisions is enhanced close to threshold. The produced off-shell antikaons propagate in the medium according to Eqs. (8), (9), and (12). According to these equations, antikaons, which are lighter than the pole mass, lose momentum and the p_T spectrum softens [75].

For the K^+ we simply assume that, in the medium, it is subject to a repulsive potential, which increases linearly with the nuclear density [19]. This increases effectively the K^+ mass. Therefore, K^+ production is suppressed in heavy-ion collisions and the p_T spectrum becomes harder [75].

We also note that, in the present study, the realization of the interaction of a K^- with a Δ baryon has been improved; consequently, the antikaon yield is slightly suppressed compared with our previous results in Ref. [75]. However, this is compensated by the decay of ϕ mesons, whose yield is enhanced by including the novel meson-baryon channels through the T-matrix approach as well as by the collisional broadening of ϕ widths.

To pin down the influence of medium effects, we consider different in-medium scenarios for the ϕ meson and for strange K, $\bar{K}$ mesons

(I) with and without including collisional broadening of ϕ mesons as discussed in Sec. II;

(II) with and without including the in-medium effects for the K and $\bar{K}$ as described in details in Ref. [75]:

   (1) *With in-medium effects for the K and $\bar{K}$*

     (i) For kaons (K^+, K^0) a repulsive density-dependent potential is included which increases the kaon mass with increasing density. This yields a shift of the production threshold and modification of production and interaction cross sections.

     (ii) For antikaons (K^-, $\bar{K}^0$) the full density and temperature dependent complex self-energy within a G-matrix approach is accounted for: the modification of the antikaon masses in line with the in-medium spectral function, off-shell dispersion relations including complex self-energies, in-medium cross sections for the production and interactions, as well as the $\bar{K}$ off-shell propagation.

   (2) *Without medium effects for the K and $\bar{K}$*

     (i) For kaons (K^+, K^0) on-shell dynamics without any potential is employed and free cross sections are used;

     (ii) For antikaons (K^-, $\bar{K}^0$) on-shell dynamics using the free production cross sections in the coupled channels is used.
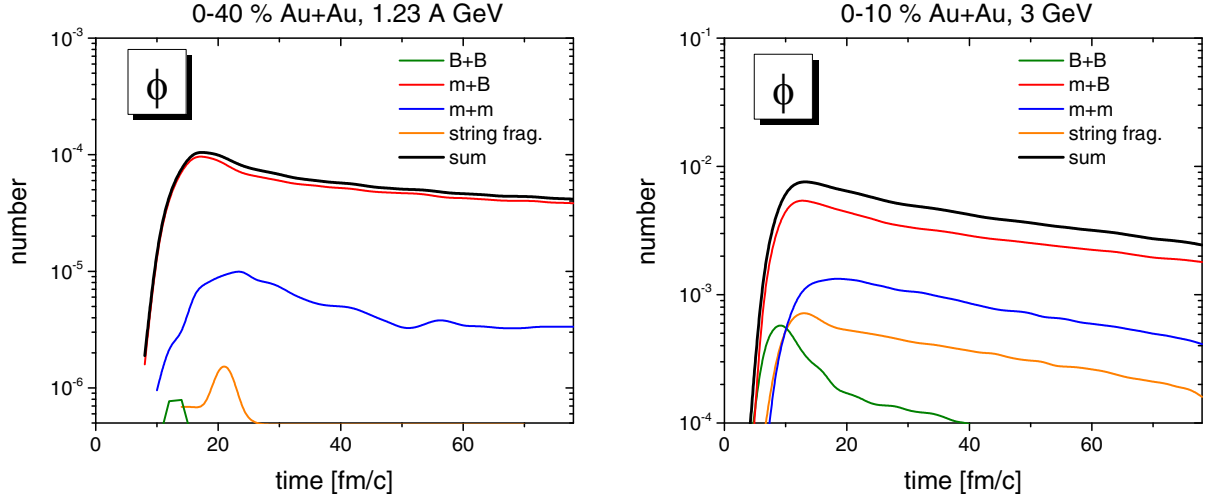
FIG. 5. Channel decomposition of the numbers of produced ϕ mesons as a function of time in Au + Au collisions, for 0%–40% centrality at $E_{\text{kin}} = 1.23A$ GeV (left) and for 0%–10% centrality at $\sqrt{s_{\text{NN}}} = 3$ GeV (right). The green, red, and blue lines show the number of ϕ mesons produced in low energy BB, mB, mm reactions, respectively, while the orange line indicates the ϕs produced by string fragmentation, the black line shows the sum of all contributions.

VI. ϕ MESON PRODUCTION IN HEAVY-ION COLLISIONS

In this section we study ϕ meson production close to the threshold by investigating Au + Au collisions at $E_{\text{kin}} = 1.23A$ GeV as measured by the HADES Collaboration as well as ϕ production above threshold, at $\sqrt{s_{\text{NN}}} = 3$ GeV, as measured by the STAR Collaboration. The PHSD calculations include the ϕ meson production channels discussed in the last section. Here we investigate the dominant channels for the ϕ meson production near and above the threshold, the time evolution of the ϕ abundances, and the rapidity distributions. Since the ϕ meson is an unstable resonance, any observables related to the ϕ mesons cannot be measured directly in experiment, rather, the ϕ mesons are reconstructed from the final K^+, K^- mesons by the invariant-mass method. The difficulty is that the kaons or antikaons can scatter elastically in the medium and the antikaon can be absorbed by inelastic collisions. Moreover, they can change their properties in the medium [75] and thus the "true" number of produced ϕ mesons and their distribution differs from the reconstructed number.

A. Channel decomposition of produced ϕ meson versus time

Figure 5 shows the number of ϕ mesons in the system as a function of time for central Au + Au collisions of the HADES experiment at $E_{\text{kin}} = 1.23A$ GeV (left) and of the STAR experiment at $\sqrt{s} = 3$ GeV (right). The PHSD calculations have been performed including the collisional broadening of ϕ mesons and taking into account the in-medium modifications of the K and $\bar{K}$ mesons.

In both cases meson-baryon reactions are the dominant channel for ϕ production. The meson-meson reactions, mainly $K + \bar{K} \rightarrow \phi$, are also very important and their contribution grows with energy due to the increasing number of strange mesons. The ϕ production in baryon-baryon collisions and by string fragmentation is subdominant. We note that $\sqrt{s} = 3$ GeV is slightly above the threshold energy for $N + N \rightarrow$

$N + N + \phi$. Therefore the contribution to the ϕ production from baryon-baryon scattering at $\sqrt{s} = 3$ GeV is much larger than at $E_{\text{kin}} = 1.23A$ GeV, but not dominant due to the small cross sections near threshold, as shown in Fig. 2. Since the ϕ decays into a kaon-antikaon pair or three pions, the number of ϕ decreases with time after the stage of initial production. This decay is stronger in a nuclear medium because of the broadened width.

B. Mass distribution of ϕ mesons

Since the ϕ mesons are unstable particles they cannot be measured directly and have to be reconstructed by their decay product using the invariant-mass method. ϕ mesons decay dominantly to kaon-antikaon pairs ($\phi \rightarrow K^0\bar{K}^0$; K^+K^-), which makes their reconstruction experimentally difficult since the kaons and antikaons suffer from final-state interactions with other mesons and baryons in the expanding hadronic matter, i.e., they can rescatter or be absorbed by surrounding hadrons. The consequences are shown in Fig. 6 which presents the invariant-mass distribution of ϕ mesons, reconstructed from K^+K^- pairs and divided by the branching ratio Br($\phi \rightarrow K^+K^-$), in Au + Au collisions at $E_{\text{kin}} = 1.23A$ GeV (left) and at $\sqrt{s_{\text{NN}}} = 3$ GeV (right). The light-blue solid lines indicate all possible combinations of $K\bar{K}$ pairs corrected by branching ratio [$K\bar{K} \equiv (K^+K^-)/\text{Br}(\phi \rightarrow K^+K^-)$] per event at the end of the PHSD calculations employing the in-medium effects for ϕ and K, $\bar{K}$. This means that each K^- has been correlated with all K^+ from the same event. This provides an estimate for the combinatorial background. The blue dashed lines shows all ϕ mesons which decayed to K^+K^- pairs at the space-time point of their decay, i.e., the ϕ mass distribution. It can be larger than the light-blue line because after the decay the (anti-)kaons can rescatter.

The red solid lines depict the ϕ's reconstructed from the final $K\bar{K}$ pairs for the case of collisional broadening of ϕ
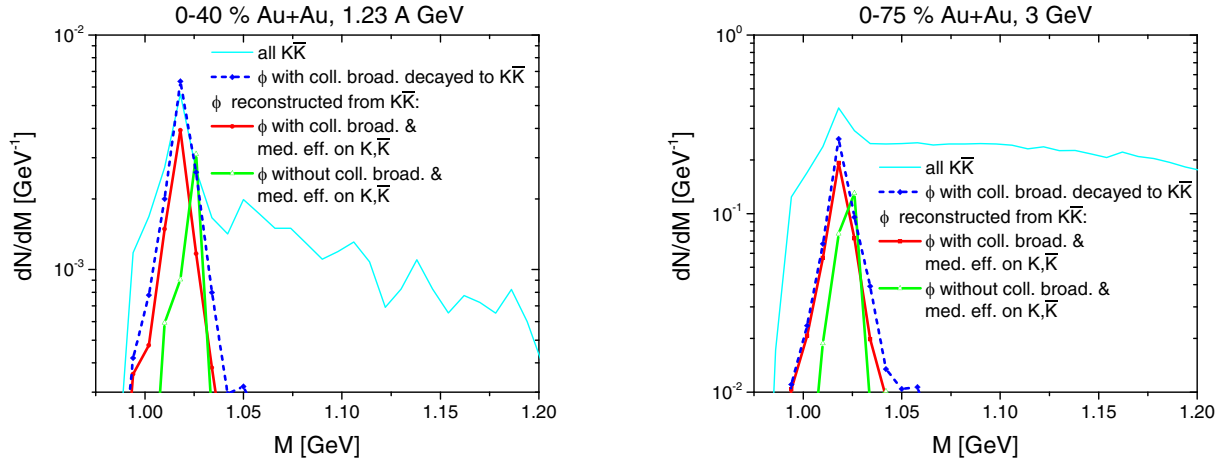
FIG. 6. Invariant-mass distribution of ϕ mesons created in Au + Au collisions at $E_{\text{kin}} = 1.23A$ GeV (left) and at $\sqrt{s_{\text{NN}}} = 3$ GeV (right). The light-blue solid lines indicate all possible combinations of $K\bar{K}$ pairs corrected by branching ratio $[K\bar{K} \equiv (K^+K^-)/Br(\phi \to K^+K^-)]$ per event at the end of the PHSD calculations with the in-medium effects for ϕ and K, $\bar{K}$. The blue dashed lines shows, at the space-time point of the decay, all ϕ mesons (with in-medium effects for ϕ and K, $\bar{K}$) which decayed into $K\bar{K}$ pairs. The red solid lines depict the ϕ's reconstructed from the final $K\bar{K}$ pairs for the case of collisional broadening of ϕ and in-medium effects for K, $\bar{K}$ mesons, while the green lines show the reconstructed ϕ's for the calculation without medium effects for the ϕ, K, $\bar{K}$ mesons. The number of reconstructed ϕ from K^+K^- pairs, divided by the branching ratio $Br(\phi \to K^+K^-)$.

and in-medium effects for the K, $\bar{K}$ mesons, while the green lines show the reconstructed ϕ's for the case without medium effects for the ϕ, K, $\bar{K}$ mesons. At each energy the number of decayed ϕ's (blue dashed lines) is larger than the number of ϕ's reconstructed from $K\bar{K}$ (red solid lines). This reduction of the reconstructed ϕ mesons compared with the true decayed ϕ's is related to the final-state interactions of (anti-)kaons by inelastic reactions—absorption or charge-exchange reactions. We note that in our theoretically "reconstructed" ϕ's we have accounted all final K^+K^- pairs coming from true ϕ decays, even if one (or both) of the decay products rescatter elastically. Because elastic collisions—with a usually small momentum transfer—do not change substantially the invariant mass of the K^+K^- pairs, this theoretical ϕ reconstruction is the closest to the experimental procedure to identify ϕ's.

The light-blue line and the red line differ due to the background [(anti-)kaons which do not come from a ϕ decay] which contributes only to the light blue line. One can see from Fig. 6 that the total number of $K\bar{K}$ pairs (light-blue line) is much larger in Au + Au collisions at $\sqrt{s} = 3$ GeV than at $E_{\text{kin}} = 1.23A$ GeV due to the opening of multiple channels for the K, $\bar{K}$ production with increasing energy. On the other hand, the number of ϕ's (true decayed and reconstructed from the final $K\bar{K}$ pairs) also grows with energy.

One sees also the large effect of the collisional broadening of ϕ mesons, green lines versus red lines, which leads to the widening of dN/dM distribution if medium effects are included compared with the case of no in-medium effects.

C. Channel decomposition of the rapidity distribution of reconstructed ϕ mesons

The rapidity distribution of the reconstructed ϕ mesons, separated by the production channels, are presented in Fig. 7

for Au + Au collisions for 0%–40% centrality at $E_{\text{kin}} = 1.23A$ GeV (left) and for 0%–10% centrality at $\sqrt{s_{\text{NN}}} = 3$ GeV (right). All PHSD calculations are performed including collisional broadening of ϕ and in-medium effects for K, $\bar{K}$ mesons. The olive, red, and green lines show the number of ϕ mesons produced in low energy BB, mB, mm reactions, respectively, while the black line shows the sum of all contributions. The dominant contribution for the ϕ production comes from meson-baryon scattering. We find that $\eta + N \to \phi + N$ (indicated by the dashed red lines) and $\rho + \Delta \to \phi + N$ (the dash-dotted magenta lines), both calculated by the T-matrix approach (Sec. IV), are most important at the energies considered here.

The blue dotted lines show the dN/dy of ϕ mesons at space-time point of their decay. They include those ϕ mesons, which could not be reconstructed experimentally (as discussed in the previous Sec. VI B) due to the final-state interaction of one of the decay products with the hadronic medium. Comparing the blue dotted and red solid lines, we find that about 60% of the ϕ mesons can be reconstructed in 0%–40% central Au + Au collisions at $E_{\text{kin}} = 1.23A$ GeV and about 70% in 0%–75% central Au + Au collisions at $\sqrt{s_{\text{NN}}} = 3$ GeV.

Supplementary to Fig. 7, in Fig. 8 we display the accumulated rapidity distribution for the ϕ production (top) and absorption (bottom) by nucleons (left) and by Δ resonances (right), separated for each meson-baryon channel from our T-matrix approach, in 0%–75% central Au + Au collisions at $\sqrt{s_{\text{NN}}} = 3$ GeV. Since hyperons are rare compared with nucleons or Δ's, the contribution from $K + Y \to \phi + N$ is less relevant in spite of the larger cross section (see Fig. 4). The most dominant channels are therefore $\eta + N \to \phi + N$ and $\rho + \Delta \to \phi + N$. Although the number of nucleons is larger than that of Δ's, $\rho + \Delta \to \phi + N$ is more dominant than $\rho + N \to \phi + N$ since the cross section for the latter is
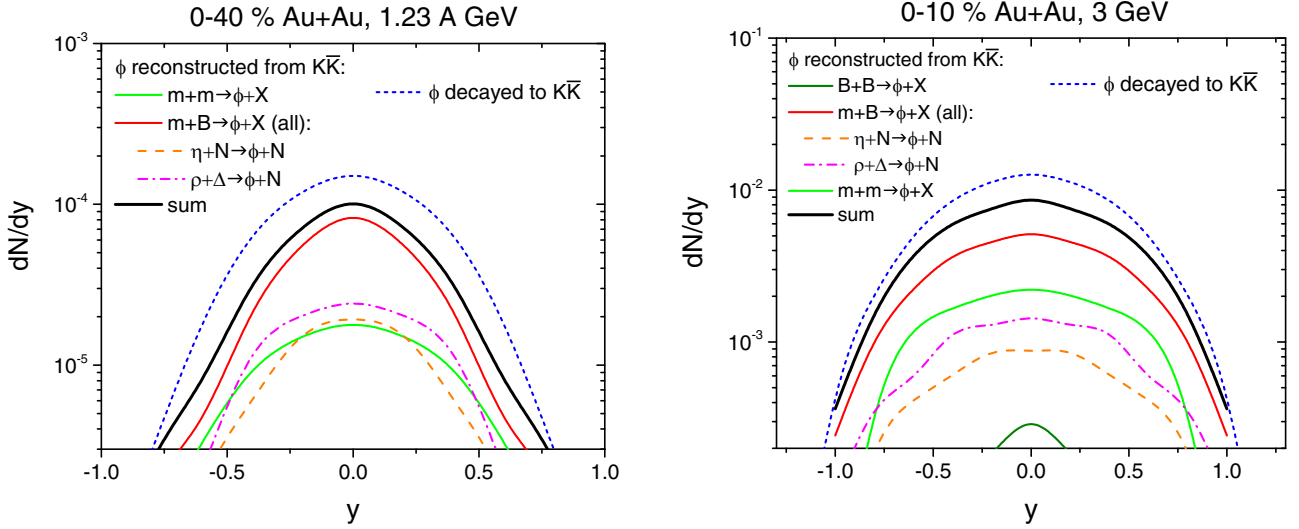
FIG. 7. Channel decomposition of the rapidity distribution of reconstructed ϕ mesons in Au + Au collisions for 0%–40% centrality at $E_{\mathrm{kin}} = 1.23A$ GeV (left) and for 0%–10% centrality at $\sqrt{s_{NN}} = 3$ GeV (right). The olive, red, and green lines show the number of ϕ mesons produced in low-energy BB, mB, mm reactions, respectively, while the black line shows the sum of all contributions. The dominant mB contributions are specified explicitly: the dashed red line shows the contribution from $\eta + N \rightarrow \phi + N$ and the dashed-dotted magenta lines indicate $\rho + \Delta \rightarrow \phi + N$ contributions. The blue dotted lines display dN/dy of ϕ's at their space-time decay points. All PHSD calculations are performed, including collisional broadening of ϕ mesons and in-medium effects for K, $\bar{K}$ mesons. The number of reconstructed ϕ from K^+K^- pairs, divided by the branching ratio Br($\phi \rightarrow K^+K^-$).

smaller and kinetically suppressed due to the smaller mass of nucleon as compared with that of the Δ. On the other hand, $\phi + N \rightarrow K + Y$ is the dominant channel for ϕ absorption due to its large cross section.

D. Comparison of ϕ meson production with experimental data

Figures 9 and 10 show the PHSD results for the rapidity distribution of reconstructed ϕ mesons from the decay into K^+K^- pairs compared with the experimental data from the HADES and STAR Collaborations. The short dashed orange lines show the PHSD results without including of the novel mB channels from the T-matrix approach and without any in-medium modification of ϕ and K, $\bar{K}$ mesons. That was the "old" setup for ϕ production in PHSD, which underestimated substantial the measured experimental data for Au + Au collisions at 1.23A GeV and 3 GeV. All other lines demonstrate the influence of the in-medium effects when the T-matrix mB channels are included: the dash-dotted lines show the results without in-medium modifications of ϕ and K, $\bar{K}$ mesons. One can see that only including the novel mB channels leads to a substantial enhancement of the ϕ yields, which, however, are below the experimental data. Furthermore, we show the influence if we include the in-medium modification of K, $\bar{K}$: the dashed lines indicate the ϕ rapidity distributions with ϕ collisional broadening, but without in-medium effects for K, $\bar{K}$ mesons. The solid lines depict the results with collisional broadening for ϕ mesons and with in-medium modifications of K, $\bar{K}$ mesons. Comparing the dashed and solid lines, no significant effect of in-medium modifications of K, $\bar{K}$ mesons on ϕ production is observed. The reason is that the main production channel of ϕ mesons is not $K + Y$, but $\eta + N$ and $\rho + \Delta$ scattering. On the other hand, the consequences of the

in-medium modification of ϕ meson by including collisional broadening are clearly visible. Since the broadening of the ϕ meson spectral function enhances the ϕ production, the dot-dashed lines are always below the solid and dashed lines.

Thus, as follows from Figs. 9 and 10, including the novel mB channels, calculated within the T-matrix of SU(6) coupled-channel approach, as well as the collisional broadening of the ϕ spectral function, PHSD reproduces the ϕ production in Au + Au collisions at $E_{\mathrm{kin}} = 1.23A$ GeV without introducing the unobserved decay of high mass baryonic resonances to ϕ mesons as proposed in other approaches [70,72]. This shows the importance of the meson-baryon channels for ϕ production incorporated in PHSD, which are absent or different in strength in the other approaches. We note that mB channels are accessible only theoretically. The T-matrix approach based on the extended SU(6) coupled-channel approach provides the presently best framework to take them into account.

Additionally to the rapidity distributions, we show in Fig. 11 for 4 rapidity bins the m_T spectra of reconstructed ϕ mesons in 0%–10% (left) and 10%–40% (right) central Au + Au collisions at $\sqrt{s_{NN}} = 3$ GeV in comparison with experimental data from the STAR Collaboration [67]. The calculations are done with the collisional broadening of ϕ mesons; the dashed lines show the results without in-medium effects for K, $\bar{K}$ mesons, while the solid lines show that with in-medium effects. The PHSD calculations approximately reproduce the slope of the m_T spectra of ϕ mesons while the yield is underestimated with collisional broadening scenario as follows from Fig. 10. One can see again that the influence of in-medium effects for K, $\bar{K}$ mesons is relatively small, as explained above.
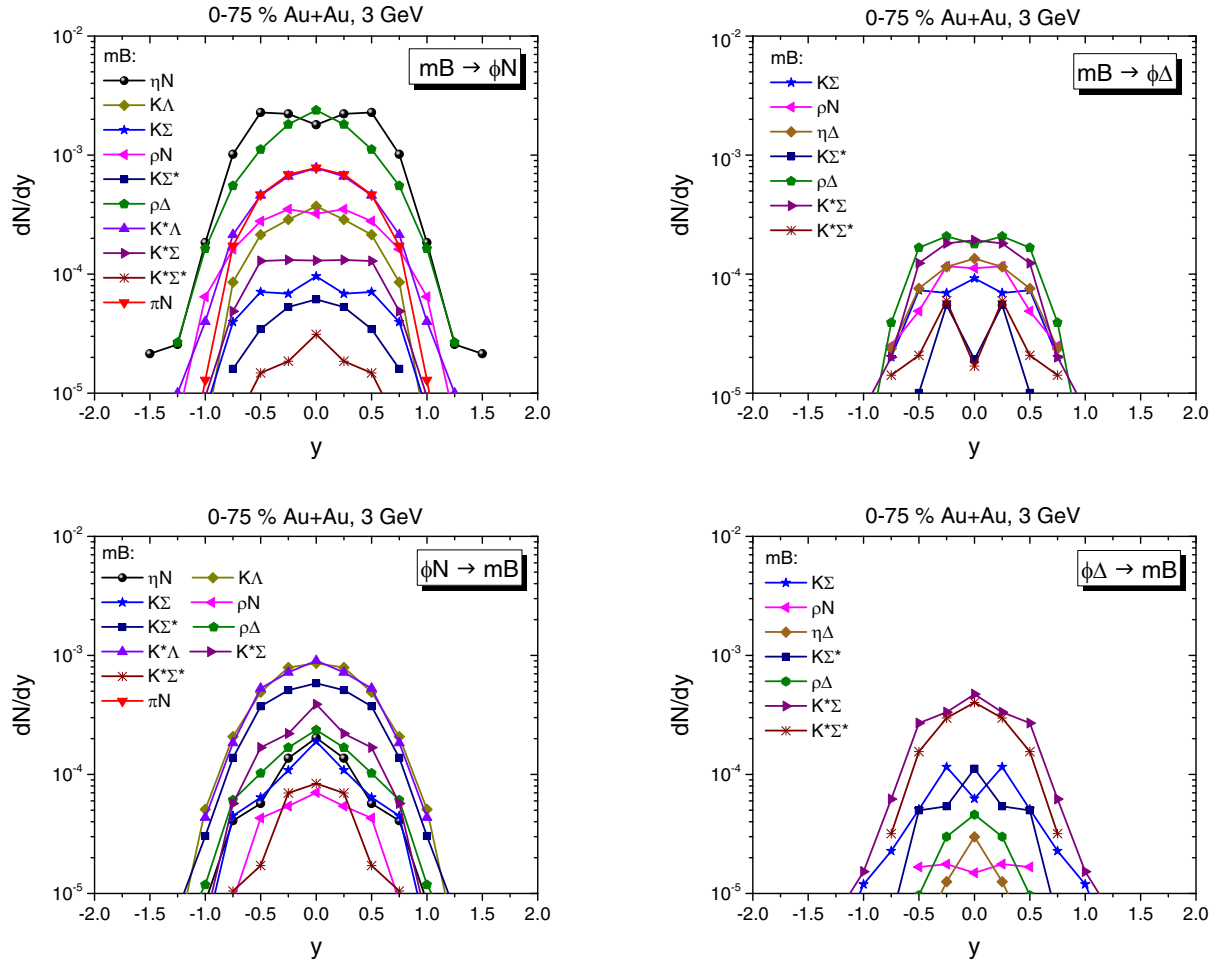
FIG. 8. (top) Channel decomposition of ϕ mesons production in $mB \to \phi N$ (top left) and in $mB \to \phi\Delta$ reactions (top right) in 0%–75% central Au + Au collisions at $\sqrt{s_{NN}} = 3$ GeV. (bottom) Channel decomposition of ϕ meson absorption by $\phi N \to mB$ (bottom left) and by $\phi\Delta \to mB$ reactions (bottom right). The individual channels, depicted in the legend, show the PHSD results for the novel $mB \leftrightarrow \phi B$ channels from the T-matrix approach. All PHSD calculations are performed for the case of collisional broadening of ϕ's and in-medium effects for K, $\bar{K}$ mesons.

In spite that the PHSD results are comparable to the HADES data for Au + Au collisions at $E_{\rm kin} = 1.23A$ GeV, the PHSD overestimates the ϕ production in Ag + Ag collisions at $E_{\rm kin} = 1.58A$ GeV when the collisional broadening of ϕ's is included. On the other hand, the STAR data on Au + Au collisions at $\sqrt{s_{NN}} = 3$ GeV are slightly underpredicted for both 0%–10% and 10%–40% centrality, although the collisional broadening of ϕ mesons is taken into account.

The PHSD offers the opportunity to investigate how in-medium effects, acting on ϕ and on (anti-)kaon, which will be briefly described in the next section, affect the ϕ meson production in heavy-ion collisions.

VII. INFLUENCE OF NEW MECHANISMS OF ϕ MESON PRODUCTION ON THE (ANTI-)KAON DYNAMICS

The enhanced ϕ production discussed above has consequences for the (anti-)kaon dynamics due to the coupling of the hidden and open strange hadrons. This coupling is more

pronounced for the $\bar{K}$ mesons since, at low energies, $\bar{K}$'s are more rarely produced compared with K's, i.e., the "feed down" from ϕ decay to $\bar{K}$ is more visible than that to K mesons. Here we investigate this impact by studying the channel decomposition for K^- production as well as by comparing the PHSD calculations for different in-medium scenarios with experimental data.

Figure 12 shows the channel decomposition of the K^- yield as a function of time in 0%–40% central Au + Au collisions at $E_{\rm kin} = 1.23A$ GeV. In-medium effects for the ϕ, K, $\bar{K}$ are included in the PHSD calculations. The dominant contributions are hyperon-meson and meson-meson scattering. The contribution from ϕ meson decay (red solid line) is similar to that from the isospin exchange $\bar{K}^0 \to K^-$. The contribution from $\phi \to K^+ K^-$ is much larger than in our previous work [75] since we are now equipped with the T-matrix approach to describe the production of ϕ mesons through meson-baryon scattering. We mention that only a part of the ϕ mesons decay to K^+ and K^-. Therefore, to obtain the total number of ϕ mesons, one has to divide those
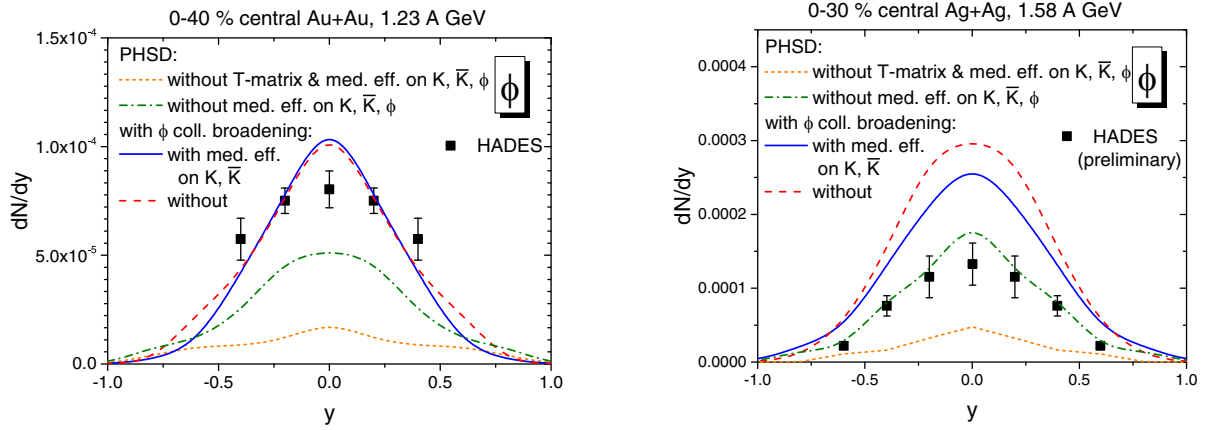
FIG. 9. Rapidity distribution of reconstructed ϕ mesons in 0%–40% central Au + Au collisions at $E_{kin} = 1.23A$ GeV in comparison with experimental data from the HADES Collaboration [64] and in 0%–30% central Ag + Ag collisions at $E_{kin} = 1.58A$ GeV in comparison with preliminary HADES data [124]. The short dashed orange lines show the PHSD results without including the novel mB channels from the T-matrix approach and without any in-medium modifications of ϕ and K, $\bar{K}$ mesons. The dash-dotted green lines show the results without in-medium modifications of ϕ and K, $\bar{K}$ mesons. The dashed red lines indicate the ϕ rapidity distributions with ϕ collisional broadening but without in-medium effects for K, $\bar{K}$ mesons. The solid blue lines show the results with collisional broadening for ϕ mesons and with in-medium modifications of K, $\bar{K}$ mesons. The number of ϕ mesons, reconstructed from K^+K^- pairs, is divided by the branching ratio Br($\phi \to K^+K^-$).

obtained from reconstructed K^+K^- pairs by the branching ratio Br($\phi \to K^+K^-$). Moreover, about 20% of the decays $\phi \to K^+ + K^-$ take place after 100 fm/c and are therefore not shown in Fig. 12.

Figure 13 shows the transverse mass spectra of $K^\pm$ calculated without and with in-medium effects for (anti-)kaon production in Au + Au collisions at $E_{kin} = 1.5A$ GeV and at different centralities. The experimental data from the KaoS Collaboration for K^+ as well as those for K^- are well reproduced by PHSD. Comparing the dashed and solid lines, we

see that in-medium effects suppress the K^+ production but enhance the K^- production, especially in central collisions where the nuclear density is higher. The in-medium effects also harden the m_T spectra of K^+ due to the repulsive potential and soften the K^- spectra.

In Fig. 14 we show the midrapidity m_T spectra of final K^- (green lines) and ϕ mesons (purple lines), calculated with (solid lines) and without (dashed lines) in-medium effects, for (anti-)kaon production in Au + Au collisions at $E_{kin} = 1.23A$ GeV, in comparison with the experimental data from
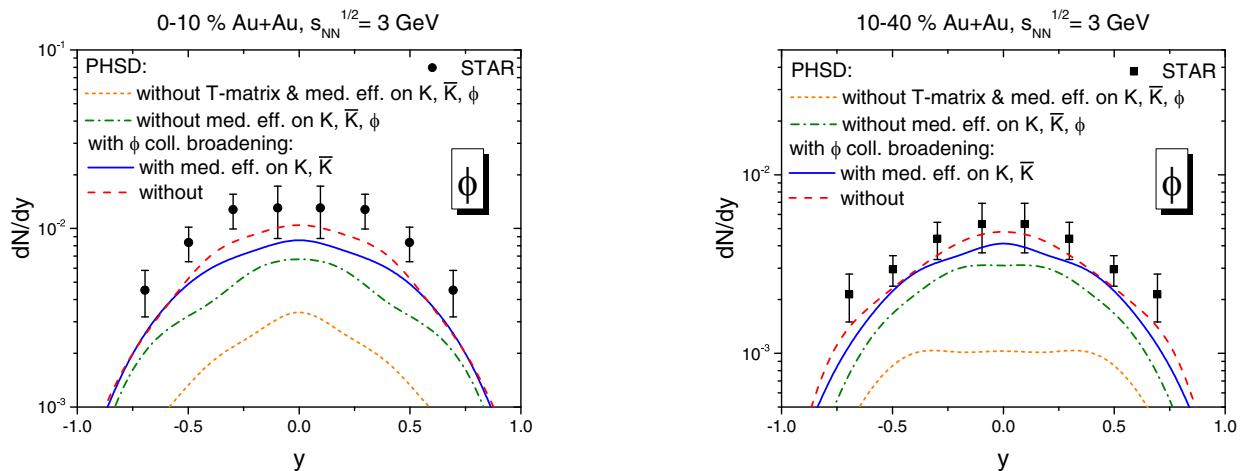

FIG. 10. Rapidity distribution of reconstructed ϕ mesons in 0%–10% (left) and 10%–40% (right) central Au + Au collisions at $\sqrt{s_{NN}} = 3$ GeV in comparison with experimental data from the STAR Collaboration [67]. The short dashed orange lines show the PHSD results without including the novel mB channels from our T-matrix approach and without any in-medium modification of ϕ and K, $\bar{K}$ mesons. The dash-dotted green lines show the results without in-medium modifications of ϕ and K, $\bar{K}$ mesons. The dashed red lines indicate the ϕ rapidity distributions with ϕ collisional broadening but without in-medium effects for K, $\bar{K}$ mesons. The solid blue lines depict the results with collisional broadening for ϕ mesons and with in-medium modifications of K, $\bar{K}$ mesons. The number of ϕ mesons, reconstructed from K^+K^- pairs, is divided by the branching ratio Br($\phi \to K^+K^-$).
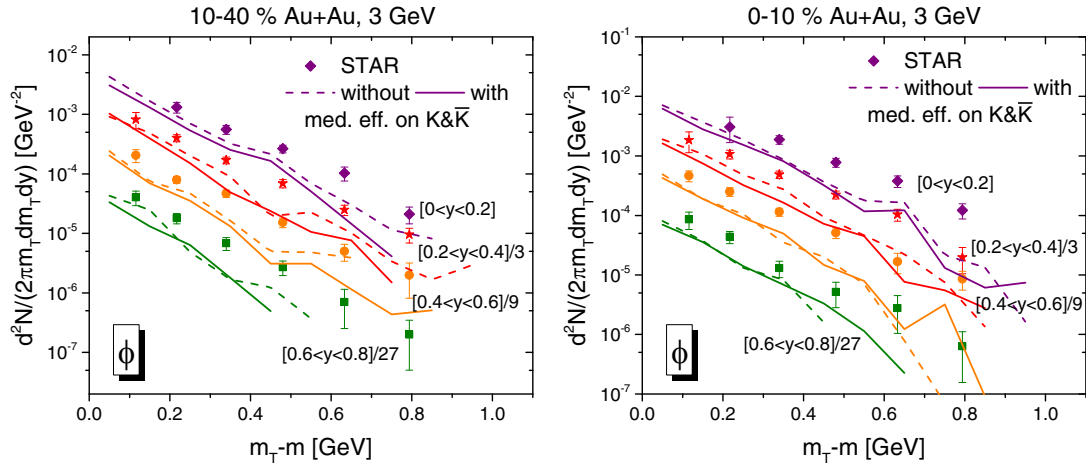
FIG. 11. m_T spectra of reconstructed ϕ mesons in 0%–10% (left) and 10%–40% (right) central Au + Au collisions at $\sqrt{s_{NN}} = 3$ GeV in comparison with experimental data from the STAR Collaboration [67]. The number of ϕ mesons, reconstructed from K^+K^- pairs, is divided by the branching ratio Br($\phi \to K^+K^-$). The calculations are done with the collisional broadening of ϕ mesons and presented for four rapidity bins $0 \leqslant y \leqslant 0.2$, $0.2 \leqslant y \leqslant 0.4$ scaled by a factor 1/3 for better visualization, $0.4 \leqslant y \leqslant 0.6$ scaled by a factor 1/9, and $0.6 \leqslant y \leqslant 0.8$ scaled by a factor 1/27. The dashed lines show the results without in-medium effects for K, $\bar{K}$ mesons, while the solid lines that with in-medium modifications of K, $\bar{K}$ mesons.

the HADES Collaboration [64]. One can see that the PHSD calculations reproduce approximately (within the achieved statistics) the measured m_T spectra of ϕ and K^- mesons. We find that the influence of the in-medium effects on the slope of the K^- spectra is rather strong—the antikaon m_T spectra with medium effects are softer than without (cf. solid and dashed green lines). On the other hand, medium effects have only a small effect on the slope of K^- stemming from the ϕ decay (orange lines) and consequently on that of the reconstructed ϕ mesons (purple lines), since the long-living ϕ mesons decay dominantly at low density. One sees also a strong difference of the slope of the final K^- spectra coming from all possible channels (as discussed above) compared with the slope of the

K^- coming from the ϕ decay, which is much softer. Thus, the ϕ contribution is softening the final K^- spectrum by enhancing the low-m_T part of the spectrum. The same tendency has been reported by the HADES Collaboration in Ref. [64], where the data have been interpreted by a two-component model: a feed down from the ϕ mesons—coming on a top of a "direct thermal" component—has been considered as a possible origin for the softening of the antikaon spectrum. We stress that, in our model, the influence of the in-medium effects on the final slope of K^- is large. Thus, the final slope of K^- is defined by the in-medium effects together with a contribution from the ϕ meson decay (which soften the K^- spectra in the same way for both scenarios—with and without medium effect).

In Fig. 15 we display the rapidity distributions of $K^+(K_s^0)$ (left column) and K^- (right column) for 0%–40% central Au + Au collisions at $E_{kin} = 1.23A$ GeV (upper row), for 0%–10%, 10%–20%, and 20%–30% central Ag + Ag collisions at $E_{kin} = 1.58A$ GeV (middle row) and for Ni + Ni collisions at $E_{kin} = 1.93A$ GeV for $b < 4.5$ fm (lower row). The PHSD results are compared with the KaoS and HADES data from Refs. [22,64], although Ag + Ag data from HADES are preliminary [127]. The solid blue and dashed red lines show the calculations with and without in-medium effects for K, $\bar{K}$; the collisional broadening of ϕ mesons is accounted for in both cases.

Compared with our previous results, Ref. [75], these calculations include the (anti-)kaons from the ϕ decay, whose production is enhanced due to the novel meson-baryon channels. However, the rapidity distributions of K^+ and K^- for Au + Au collisions at $E_{kin} = 1.23A$ GeV (upper row) and for Ni + Ni collisions at $E_{kin} = 1.93A$ GeV (lower row) are similar to our previous calculations [75] since the "feed down" from ϕ mesons to the K^+ yield is very small compared with other kaon production channels; the K^- production is slightly
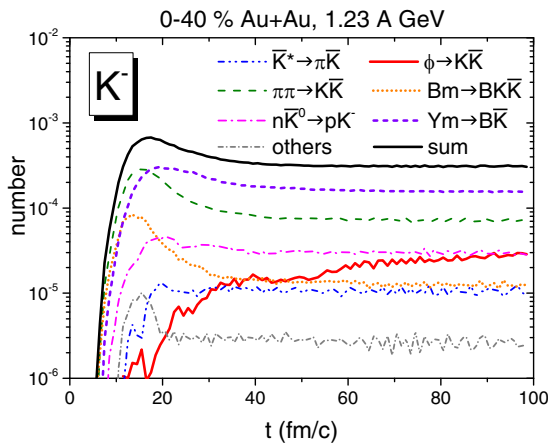

FIG. 12. Channel decomposition of the K^- yield for 0%–40% central Au + Au collisions at $E_{kin} = 1.23A$ GeV as a function of time. The individual channels are depicted in the legend. The solid red line shows the contribution from the $\phi \to K^+K^-$ decay. The PHSD calculations are performed including ϕ and (anti-)kaon in-medium effects.
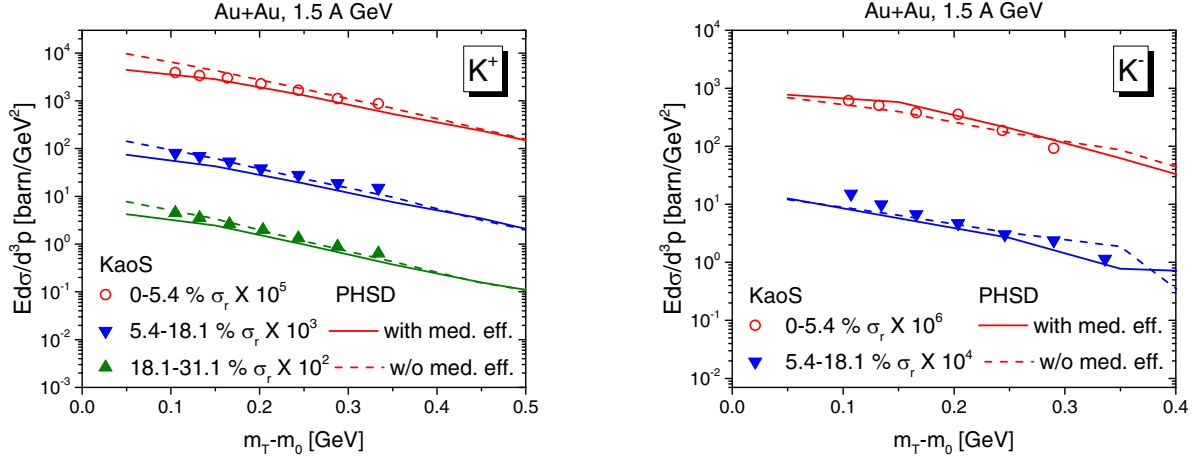
FIG. 13. m_T spectra of K^+ (left) and K^- (right) calculated with and without in-medium effects for (anti-)kaon production in Au + Au collisions at $E_{\text{kin}} = 1.5A$ GeV, in comparison with experimental data from the KaoS Collaboration [125].

enhanced from ϕ meson decay, however, it is compensated by the enhanced K^- absorption by Δ baryons. The contribution of the ϕ meson decay to K^- production we will discuss in the next section. In the middle row we display the results for Ag + Ag at $\sqrt{s_{NN}} = 1.58A$ GeV for which recently preliminary experimental data on K_s^0 have been made available by the HADES Collaboration. Also here the in-medium modifications of the kaon properties are necessary to describe the experimental data. On the right-hand side we show the predictions for the K^- rapidity distribution. The upcoming HADES data will be important to investigate the system size dependence of strangeness production: as shown in Ref. [75] and confirmed now by the updated PHSD calculations, including in-medium effects, PHSD overestimates the HADES data on K^- production in Au + Au collisions at 1.23A GeV but

FIG. 14. m_T spectra at midrapidity of final K^- (green lines) and ϕ mesons (purple lines) calculated with (solid lines) and without (dashed lines) in-medium modifications for (anti-)kaon production in Au + Au collisions at $E_{\text{kin}} = 1.23A$ GeV, in comparison to the experimental data from the HADES Collaboration [64]. The number of ϕ mesons is corrected by the branching ratio.

describes, on the other hand, the KaoS, FOPI, and HADES data for lighter systems as Ni + Ni, Ar + KCl and C + C at different SIS energies including in-medium modifications. Moreover, including these in-medium effects, PHSD reproduces the K^+ experimental observables for light and heavy systems as well as experimental data on Λ production which give solid constraints on the strangeness balance in the calculations.

Also above the kinematical threshold (for p-p collisions) the experimental rapidity distribution of K^- mesons agrees well with the experimental data if in-medium effects are included. In Fig. 16 (right) we compare our calculations with the K^- rapidity distributions measured by the STAR Collaboration for 0%–10% and 10%–40% central Au + Au collisions at $\sqrt{s_{NN}} = 3$ GeV [67]. As seen, the K^- rapidity distributions are better described by including in-medium modifications of the antikaon. On the lower panel of Fig. 16 we show the m_T spectra of K^- for 0%–10% central (left) and 10%–40% central (right) Au + Au collisions at $\sqrt{s_{NN}} = 3$ GeV. The calculations are done with the collisional broadening of ϕ mesons and presented for nine rapidity bins. The dashed lines show the results without in-medium effects for K, $\bar{K}$ mesons, while the solid lines that with in-medium modifications of K, $\bar{K}$ mesons. One can see in the top right Fig. 16 that PHSD calculations with in-medium effects on K, $\bar{K}$ mesons reproduce the experimental m_T spectra rather well.

On the left part of Fig. 16 we show our predictions for the K^+ production with (solid blue line) and without (dashed red line) medium effects for 0%–5% central Au + Au collisions at $\sqrt{s_{NN}} = 3$ GeV, where the new STAR data are expected. One can see the suppression of the K^+ yield at midrapidity for the case of in-medium modifications.

Figure 17 (left) shows the PHSD results—with (solid lines) and without (dashed lines) medium effects—for the K^+ (blue) and K^- (red) rapidity distributions in Au + Au collisions at $E_{\text{kin}} = 2A$ and $4A$ GeV in comparison with the E866 data at midrapidity [128]. Also, here one can see that the experimental data for K^+ are better reproduced by calculations with
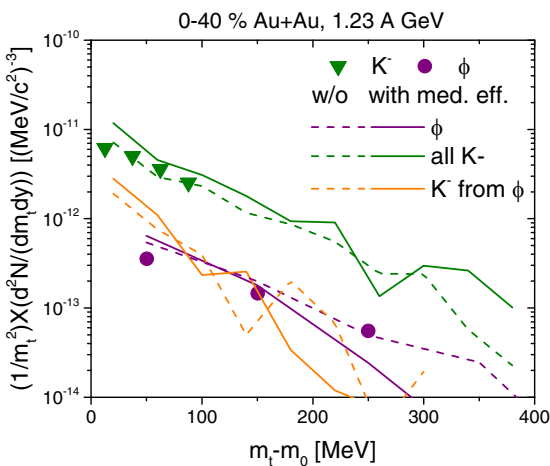
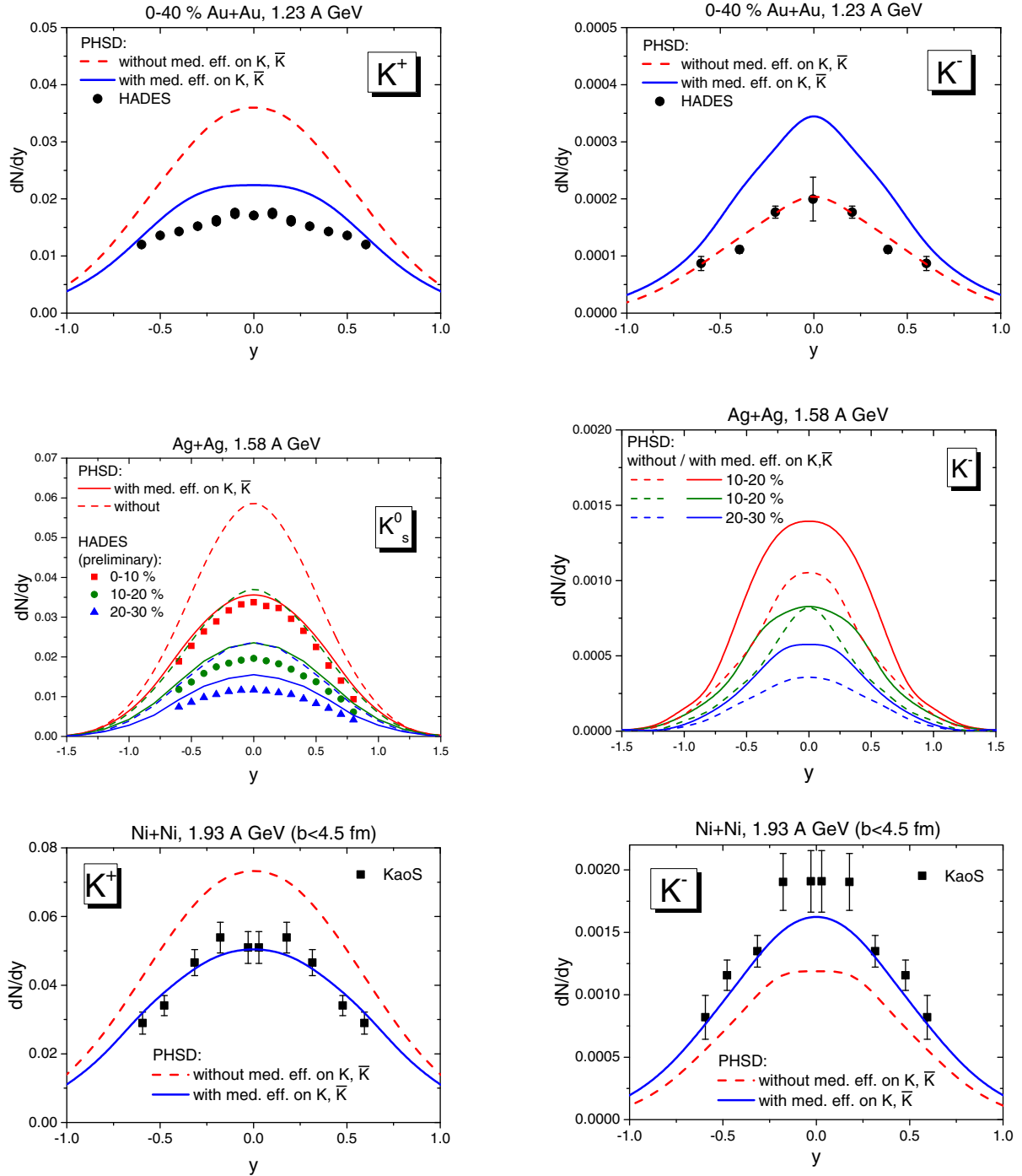FIG. 15. Rapidity distributions of $K^+(K_s^0)$ (left column) and K^- (right column) for 0%–40% central Au + Au collisions at $E_{kin} = 1.23A$ GeV (upper row), for 0%–10%, 10%–20%, and 20%–30% central Ag + Ag collisions at $E_{kin} = 1.58A$ GeV (middle row) and for Ni + Ni collisions at $E_{kin} = 1.93A$ GeV for $b < 4.5$ fm (lower row). The solid blue and dashed red lines show the PHSD calculations with and without in-medium effects for K, $\bar{K}$; the collisional broadening of ϕ mesons is accounted for in both cases. The solid symbols show the experimental data from Refs. [22,64,126] and preliminary Ag + Ag data from HADES [127].

medium effects. Moreover, the m_T spectra of K^+ mesons for central Au + Au collisions at midrapidity (shown in Fig. 17, right), clearly favor the in-medium scenario for K^+ for both energies. For the K^- mesons the in-medium effects enhance only slightly the yield at midrapidity and soften the slope of the m_T spectra at low m_T.

In Fig. 18 we show the m_T spectra of Ξ^- in 0%–10% (left) and 10%–40% central (right) Au + Au collisions at $\sqrt{s_{NN}} = 3$ GeV, compared with the experimental data from the STAR Collaboration [67]. At low energies the Ξ is produced in the PHSD through the elementary reactions $Y + Y \to \Xi + N$ and $Y + \bar{K} \to \Xi + \pi$ with cross sections calculated within
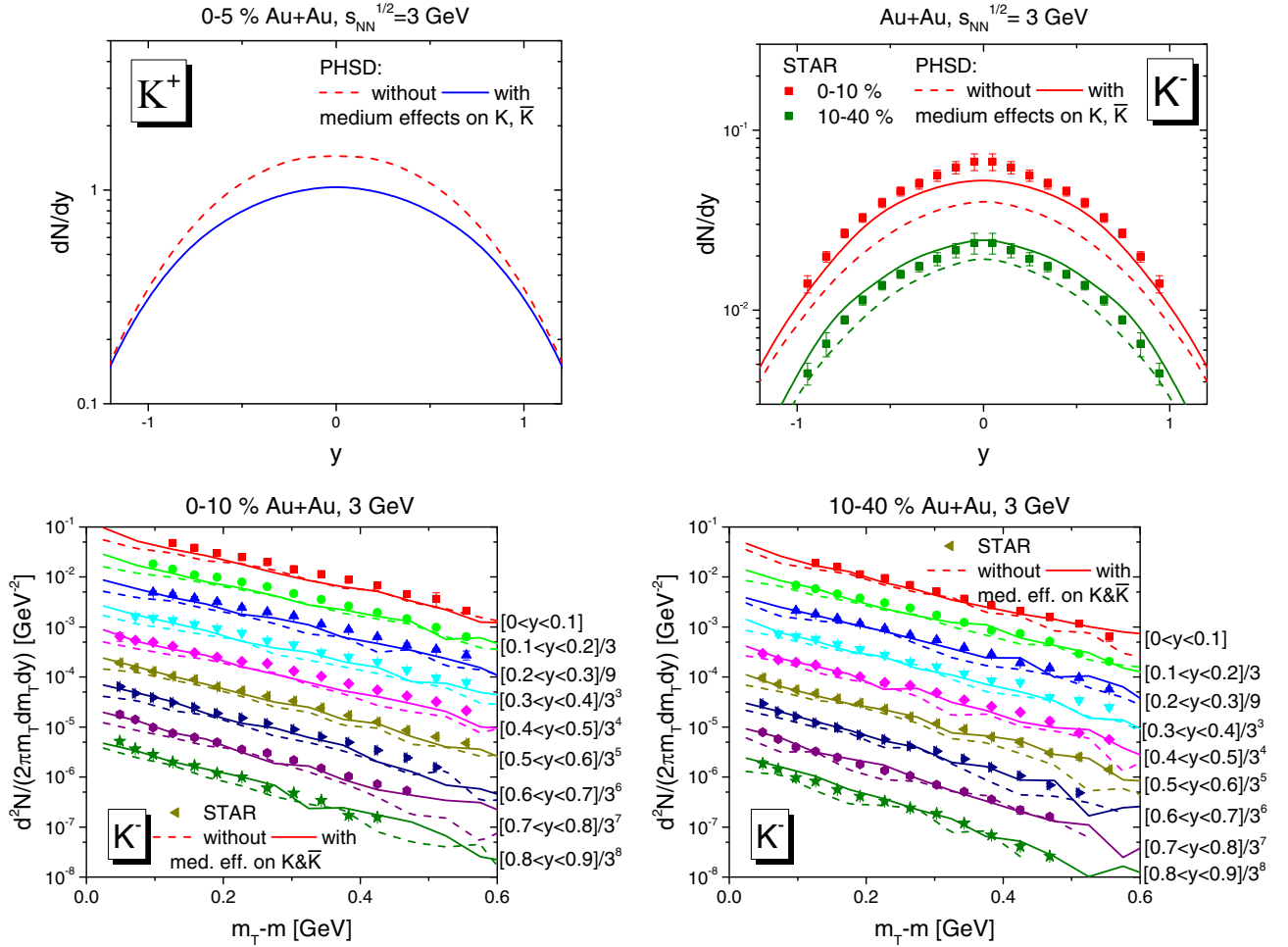
FIG. 16. Rapidity distributions of K^+ (top left) and K^- (top right) for Au + Au collisions at $\sqrt{s_{NN}} = 3$ GeV. The PHSD calculations with (solid lines) and without (dashed lines) in-medium effects on (anti-)kaon production are displayed and compared for the K^- with the preliminary data of the STAR Collaboration [67]. The K^+'s are calculated for 0%–5% centrality, while K^- mesons are calculated and compared for two centrality classes: for 0%–10% (red) and 10%–40% (green) central Au + Au collisions. The m_T spectra of K^- for 0%–10% central (bottom left) and 10%–40% central (bottom right) Au + Au collisions at $\sqrt{s_{NN}} = 3$ GeV. The calculations are done with the collisional broadening of ϕ mesons and presented for 9 rapidity bins $0 \leqslant y \leqslant 0.1$, $0.1 \leqslant y \leqslant 0.2$, ..., $0.8 \leqslant y \leqslant 0.9$, scaled by a factor $1/3$ each for better visualization. The dashed lines show the results without in-medium effects for K, $\bar{K}$ mesons, while the solid lines that with in-medium modifications of K, $\bar{K}$ mesons.

the model of Refs. [129–131]. The inverse reactions are implemented by detailed balance. At high energies, the Ξ^-s are produced via string fragmentation. The calculations are done with the collisional broadening of ϕ mesons for four rapidity bins. The dashed lines show the results without in-medium effects for K, $\bar{K}$ mesons, while the solid lines that with in-medium modifications of K, $\bar{K}$ mesons. One sees that the PHSD spectra are consistent with the experimental data (within the achieved statistics). The in-medium modifications of (anti)kaons leads to the reduction of the Ξ^- yield, since hyperons are less produced with the medium effects.

VIII. STRANGE-PARTICLE RATIOS

In this section we show the PHSD results for the ratios of strange particles K^-/K^+, ϕ/K^-, and $\phi/\Xi-$ based on the results presented in Secs. VI and VII.

In Fig. 19 we present the PHSD results for the K^-/K^+ ratio calculated with (solid blue line) and without (dashed red line) in-medium effects for (anti-)kaon production in $A + A$ collisions versus the beam energy E_{beam} in comparison with the experimental data of Refs. [64,125]. We note that the K^-/K^+ ratio is rather flat as function of centrality, therefore one can simply look at the ratio in different systems and centrality classes. As follows from Fig. 19 the experimental data are in favor of the in-medium scenario for the increasing K^-/K^+ ratio. Only the HADES data for Au + Au at $1.23A$ GeV are overestimated due to the overestimation of the K^- yield, as discussed above. More $K^\pm$ and ϕ experimental data at the low energy and their excitation functions would be helpful to clarify the discrepancies.

Figure 20 shows the ϕ/K^- ratio as a function of the collision energy from $E_{kin} = 1.23A$ GeV to $\sqrt{s_{NN}} = 200$ GeV. The PHSD results are presented for four different

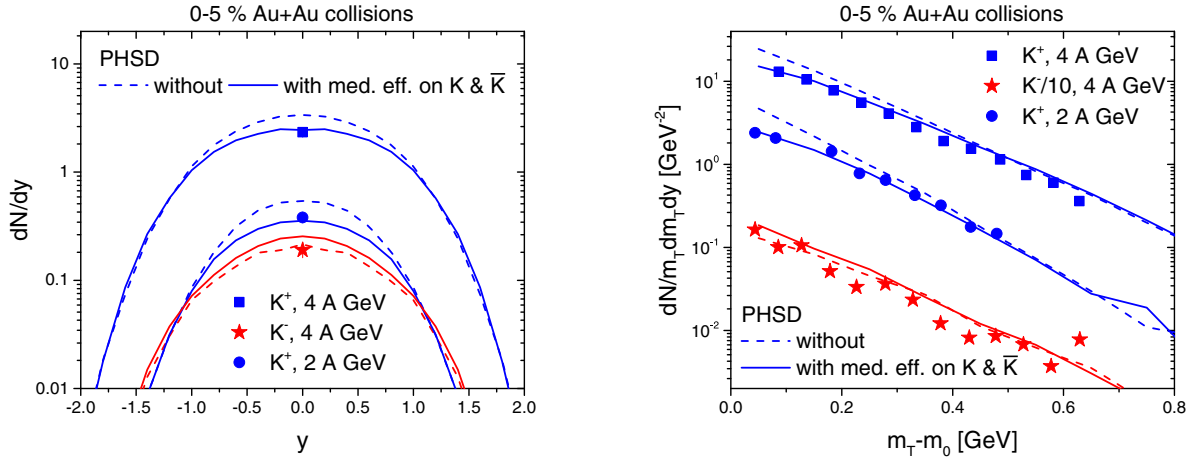FIG. 17. Rapidity distributions (left) and m_T-spectra (right) at midrapidity of K^+ (blue) and K^- (red) in 0%–5% Au + Au collisions at $E_{kin} = 2$ and 4 A GeV. The PHSD calculations with (solid lines) and without (dashed lines) in-medium effects for (anti-)kaon production are compared with the experimental data of the E866 Collaboration [128].

scenarios:

(1) The orange dashed line is the ratio without any in-medium effect and also excluding the novel mB production channels of ϕ's from the T-matrix approach. This ratio is comparable to the experimental data at high energies ($\sqrt{s_{NN}} > 20$ GeV) but underestimates significantly the experimental data at low energies [46–50,66,67].

(2) The green line shows the ϕ/K^- ratio including the novel mB channels for ϕ mesons produced from our T-matrix approach, but without in-medium effects for K, $\bar{K}$. These new mB production channels increase the ratio at low collisional energies, and the results are consistent with the experimental data down to $\sqrt{s_{NN}} = 3$ GeV. At high collisional energies the

contribution from meson-baryon scattering is not important because the dominant mechanisms for ϕ production at high energies are string fragmentation and hadronization of the quark-gluon plasma, which are dominated by phase space.

(3) In a baryon environment the width of the ϕ mesons broadens, modifying the spectral function. Including this collisional broadening (red line) the ϕ/K^- ratio becomes comparable to the experimental data at all energies.

(4) Finally, we display (by the blue line) the results if, in addition to the collisional broadening of the ϕ meson width, the in-medium modifications of the (anti-)kaon properties are taken into account. As already mentioned in the previous sections, these in-medium effects enhance the K^- production in nuclear matter
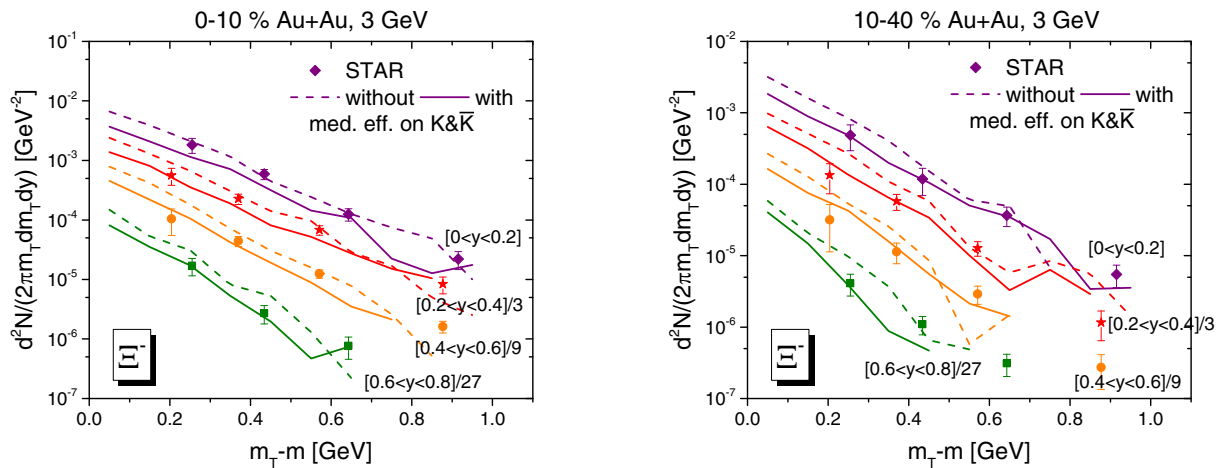

FIG. 18. m_T spectra of Ξ^- in 0%–10% (left) and 10%–40% central (right) Au + Au collisions at $\sqrt{s_{NN}} = 3$ GeV, compared with the experimental data from the STAR Collaboration [67]. The calculations are done with the collisional broadening of ϕ mesons and presented for four rapidity bins $0 \leqslant y \leqslant 0.2$, $0.2 \leqslant y \leqslant 0.4$ scaled by a factor 1/3 for better visualization, $0.4 \leqslant y \leqslant 0.6$ scaled by a factor 1/9, and $0.6 \leqslant y \leqslant 0.8$ scaled by a factor 1/27. The dashed lines show the results without in-medium effects for K, $\bar{K}$ mesons, while the solid lines that with in-medium modifications of K, $\bar{K}$ mesons.
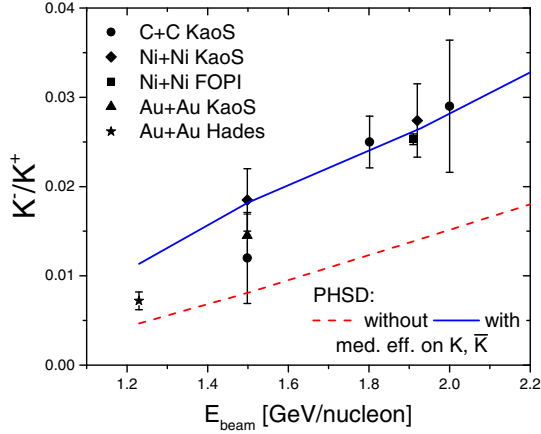
FIG. 19. The PHSD results for the ratio K^-/K^+ calculated with (solid blue line) and without (dashed red line) in-medium effects for (anti-)kaon production in $A + A$ collisions versus the beam energy E_{beam}. The symbols represent the experimental data of Refs. [64,125,132].

while the yield of the ϕ meson is not strongly affected by the in-medium modification of the (anti-)kaon. As a result, the ratio decreases due to the enhanced K^- production.

We study furthermore the ϕ/Ξ^- ratio. Figure 21 shows the ϕ/Ξ^- ratio as a function of the collision energy with (solid blue line) and without (dashed red line) in-medium effects for (anti-)kaons. The collisional broadening of the ϕ meson
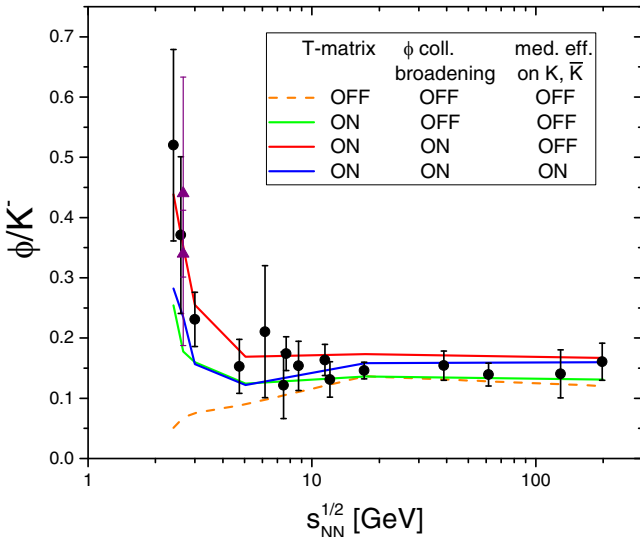
FIG. 20. The PHSD results for the ratio ϕ/K^- in midrapidity ($|y| \leqslant 0.3$) as a function of the collision energy for four different scenarios: with and without novel mB channels for the ϕ meson production from the T-matrix approach and with and without the collisional broadening of ϕ meson width and in-medium effects on (anti-)kaons (cf. the legend). The number of ϕ mesons, reconstructed from K^+K^- pairs, is divided by the branching ratio $\text{Br}(\phi \to K^+K^-)$. The solid symbols show the compilation of the experimental data from Refs. [46–50,66,67].

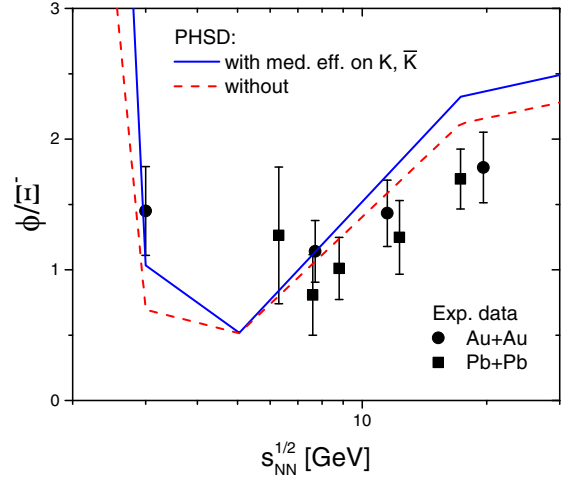FIG. 21. PHSD calculations for the ϕ/Ξ^- ratio as a function of the collision energy for calculations with (solid blue line) and without (dashed red line) in-medium effects for (anti-)kaons in comparison with the experimental data [67]. The number of ϕ mesons, reconstructed from K^+K^- pairs, is divided by the branching ratio $\text{Br}(\phi \to K^+K^-)$.

widths is included in both cases. Since the ϕ production depends little on the in-medium effects of (anti-)kaons, this ratio is insensitive to the (anti-)kaon properties. The ratio is largest at HADES energies and decreases rapidly with increasing collision energy. After a minimum it slowly increases as shown in the figure. Our calculations are consistent with the experimental data [67].

Finally, in Fig. 22 we show the ratios ϕ/K^- (upper) and ϕ/Ξ^- (lower) as a function of centrality with (solid blue line) and without (dashed red line) medium effects on (anti)kaon in Au + Au collisions at $\sqrt{s_{NN}} = 3$ GeV in comparison with experimental data from the STAR Collaboration [67]. One gets an impression that the experimental ϕ/K^- ratio is better described by the scenario without medium effect. However, looking at the ϕ and K^- spectra separately in Figs. 9 and 16, one can see that, with in-medium effects, we better describe the K^- rapidity distributions, while without in-medium effects it is substantially underestimated. On the other hand, the ϕ yield is less sensitive to the in-medium effects on K, $\bar{K}$. Thus, the ratio ϕ/K^- is larger for the scenario without in-medium effects due to the underestimation of K^- yield. For the ϕ/Ξ^- ratio the situation is opposite since the Ξ yield is smaller with in-medium effects for (anti)kaons as follows from Fig. 18, thus the ϕ/Ξ^- ratio is larger for the in-medium scenario for (anti)kaons.

IX. SUMMARY

In this study we have investigated the hidden (ϕ meson) and open (kaon and antikaon) strangeness production and their mutual dependence in heavy-ion collisions from subthreshold to relativistic energies within the microscopic off-shell PHSD transport approach. Motivated by the fact that conventional transport models, which propagate on-shell particles, cannot explain the ϕ meson yield in heavy-ion
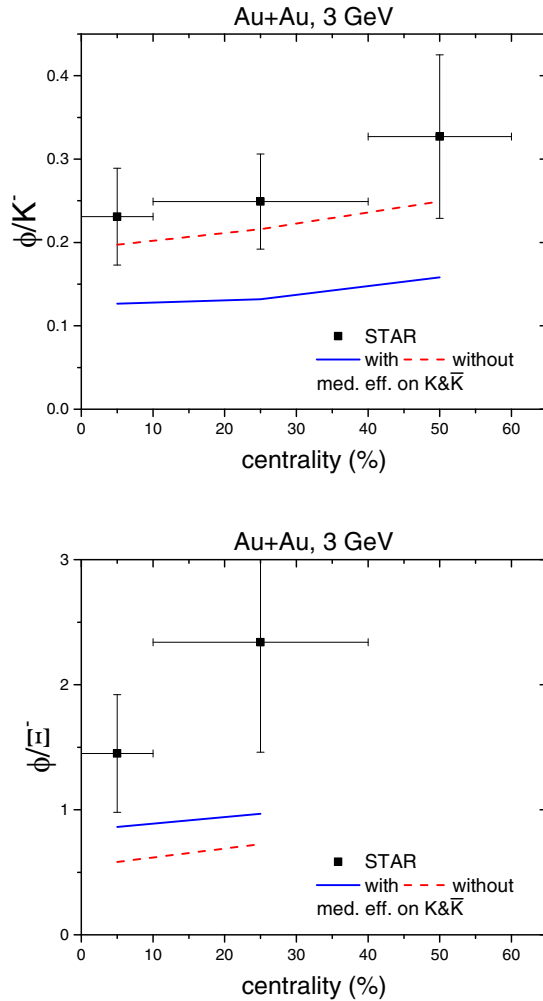
FIG. 22. Ratios ϕ/K^- (upper) and ϕ/Ξ^- (lower) as a function of centrality with (solid blue line) and without (dashed red line) medium effects on (anti)kaon in Au + Au collisions at $\sqrt{s_{NN}} =$ 3 GeV in comparison with experimental data from the STAR Collaboration [67].

reactions at low beam energies without introducing a not-observed ϕ decay of heavy baryonic resonances, we studied systematically the properties of hidden and open strange mesons in the dense and hot medium created in heavy-ion collisions and the reaction channels which contribute to the production of ϕ mesons in a nuclear environment. This includes

  (i) *The in-medium modifications of ϕ mesons.*
       Collisional broadening leads to an increase of the width of ϕ mesons, proportional to the baryon density and hence to a broadening of the ϕ meson spectral function. Consequently, the ϕ meson production threshold in all hadronic reactions is lowered if the ϕ is in a strongly interacting environment. This enhances the ϕ meson production at subthreshold energies and leads to a modification of the (elastic and inelastic) cross sections with hadrons.

Based on the off-shell Kadanoff-Baym equations, PHSD is able to change dynamically the width of the ϕ while traveling through the dense baryonic medium. This allows for a consistent transport of the ϕ meson in the dense matter which is created in heavy-ion reactions.

  (ii) *New relevant $mB \to \phi$ production channels.*
        We used the SU(6) chiral effective Lagrangian in the T-matrix approach to calculate the different meson-baryon cross sections which contribute to ϕ production. Taking into account the five sets of total quantum numbers $(I, S, J) = (1/2, 0, 1/2), (3/2, 0, 1/2),$ $(1/2, 0, 3/2), (3/2, 0, 2/2), (3/2, 0, 5/2)$, ten scattering channels to produce $\phi + N$ and seven channels to produce $\phi + \Delta$ are calculated. By this we methodically extended the usually considered $m + B$ channels involving pions, nucleons, and Δ's by accounting for s-wave scattering $m + B \to \phi + B$ reactions with $m = \eta, K, \rho, K^*$ mesons and $B = N, \Delta, \Lambda, \Sigma, \Sigma^*$ baryons for all possible $I = 1/2$ and $3/2$ channels. We have found that among them the $\eta N \to \phi N$ channel is the most important. Although the cross section is not the largest, the η abundance, larger than that for all other mesons (besides the pion), makes this channel important at SIS energies. The reverse reactions $\phi B \to mB$ have been realized by detailed balance. These mB channels have been neglected up to now in transport approaches.

 (iii) *The in-medium modifications of K and $\bar{K}$ mesons.*
        Following our previous study [75], we have accounted for the in-medium modifications of strange mesons, too: a repulsive potential for kaons which increases linearly with the baryon density and which leads to the increase of the kaon mass with increasing density while the width remains negligibly small; the density and temperature dependent complex self-energy obtained by a G-matrix approach for antikaons which leads to a substantial broadening of the spectral functions and to the decrease of the pole mass.

Our findings can be summarized as follows:

  (1) In-medium effects, as a collisional broadening of the ϕ meson spectral function, lead to an enhancement of ϕ meson production, especially at subthreshold energies, as demonstrated in Figs. 9 and 10.
  (2) The novel $mB \to \phi B$ channels from the SU(6) chiral Lagrangian in the T-matrix approach enhance considerably the ϕ production in heavy-ion collisions, see Figs. 9, 10, and 20.
  (3) Due to rescattering of the K^+ or K^- in the medium, in Au + Au reactions at energies between $E_{\mathrm{kin}} = 1.23A$ GeV and $\sqrt{s_{NN}} = 3$ GeV only 60%–70% of the decaying ϕ's can be reconstructed by the invariant-mass method.
  (4) The in-medium effects for open strange mesons— a repulsive potential for the kaons and density and temperature dependent complex self-energies from the G-matrix approach for antikaons—lead to a sizable

modification of the yield and spectra of (anti-)kaons, as already investigated in our previous study [75]. However, they also have an impact on the final ϕ meson observables: by reducing the reconstructed ϕ mesons since the number of K^+ decreases and the rescattering of K^- is getting stronger with the in-medium effects.

(5) The measured K, $\bar{K}$ rapidity and m_T distributions for different systems at SIS energies as well as the K^-/K^+ ratio favor the in-medium scenario for the (anti-)kaons, except for the Au + Au data at 1.23A GeV where we overestimate the K^- yield.

(6) The experimental ϕ/K^- ratio can be reproduced by PHSD calculations, incorporating the collisional broadening for the ϕ meson spectral function and including novel mB channels for the ϕ production. This leads to a strong enhancement of ϕ production close to threshold.

On the other hand, an inclusion of the in-medium effects for K, $\bar{K}$, which leads to a strong enhancement of the K^- yield and overestimation of Au + Au data at 1.23A GeV leads to a reduction of the ϕ/K^- ratio and an underestimation of this experimental data point while for the other energies and systems the experimental ϕ/K^- ratio is still within the low experimental error bars for the full in-medium scenario for ϕ, K, $\bar{K}$.

(7) The ratio ϕ/Ξ^- is also found to be reproduced within the PHSD approach including the full in-medium scenario for ϕ, K, $\bar{K}$ and novel mB channels for ϕ production.

[1] W. Cassing and E. L. Bratkovskaya, Phys. Rep. **308**, 65 (1999).

[2] C. Hartnack, H. Oeschler, Y. Leifels, E. L. Bratkovskaya, and J. Aichelin, Phys. Rep. **510**, 119 (2012).

[3] J. Aichelin and C. M. Ko, Phys. Rev. Lett. **55**, 2661 (1985).

[4] W. Cassing, E. L. Bratkovskaya, U. Mosel, S. Teis, and A. Sibirtsev, Nucl. Phys. A **614**, 415 (1997).

[5] C. Hartnack, H. Oeschler, and J. Aichelin, Phys. Rev. Lett. **90**, 102302 (2003).

[6] L. Tolos and L. Fabbietti, Prog. Part. Nucl. Phys. **112**, 103770 (2020).

[7] M. Bleicher and E. Bratkovskaya, Prog. Part. Nucl. Phys. **122**, 103920 (2022).

[8] D. B. Kaplan and A. E. Nelson, Phys. Lett. B **175**, 57 (1986).

[9] A. E. Nelson and D. B. Kaplan, Phys. Lett. B **192**, 193 (1987).

[10] M. Lutz, Phys. Lett. B **426**, 12 (1998).

[11] T. Waas, N. Kaiser, and W. Weise, Phys. Lett. B **365**, 12 (1996).

[12] T. Waas, N. Kaiser, and W. Weise, Phys. Lett. B **379**, 34 (1996).

[13] J. Schaffner-Bielich, V. Koch, and M. Effenberger, Nucl. Phys. A **669**, 153 (2000).

[14] M. F. M. Lutz and E. E. Kolomeitsev, Nucl. Phys. A **700**, 193 (2002).

[15] A. Ramos and E. Oset, Nucl. Phys. A **671**, 481 (2000).

[16] A. Mishra, K. Balazs, D. Zschiesche, S. Schramm, H. Stöcker, and W. Greiner, Phys. Rev. C **69**, 024903 (2004).

[17] L. Tolos, A. Ramos, A. Polls, and T. T. S. Kuo, Nucl. Phys. A **690**, 547 (2001).

[18] L. Tolos, A. Ramos, and A. Polls, Phys. Rev. C **65**, 054907 (2002).

[19] C. L. Korpa and M. F. M. Lutz, Acta Phys. Hung. New Ser.: Heavy Ion Phys. **22**, 21 (2005).

[20] D. Best *et al.* (FOPI Collaboration), Nucl. Phys. A **625**, 307 (1997).

[21] F. Laue *et al.* (KaoS Collaboration), Phys. Rev. Lett. **82**, 1640 (1999).

[22] M. Menzel *et al.* (KaoS Collaboration), Phys. Lett. B **495**, 26 (2000).

[23] C. T. Sturm *et al.* (KAOS Collaboration), Phys. Rev. Lett. **86**, 39 (2001).

[24] M. Stefanon *et al.*, Astrophys. J., Suppl. Ser. **229**, 32 (2017).

[25] V. Zinyuk *et al.* (FOPI Collaboration), Phys. Rev. C **90**, 025210 (2014).

[26] G. Agakishiev *et al.* (HADES Collaboration), Eur. Phys. J. A **47**, 21 (2011).

[27] J. Adamczewski-Musch *et al.* (HADES Collaboration), Phys. Lett. B **793**, 457 (2019).

[28] X. S. Fang, C. M. Ko, G.-Q. Li, and Y. M. Zheng, Phys. Rev. C **49**, R608 (1994).

[29] G.-Q. Li, C. M. Ko, and X. S. Fang, Phys. Lett. B **329**, 149 (1994).

[30] G.-Q. Li, C. H. Lee, and G. E. Brown, Nucl. Phys. A **625**, 372 (1997).

[31] G.-Q. Li, C. M. Ko, and B.-A. Li, Phys. Rev. Lett. **74**, 235 (1995).

[32] G.-Q. Li, C. M. Ko, and G. E. Brown, Phys. Lett. B **381**, 17 (1996).

[33] S. Pal, C. M. Ko, and Z.-w. Lin, Phys. Rev. C **64**, 042201(R) (2001).

[34] E. L. Bratkovskaya, W. Cassing, and U. Mosel, Nucl. Phys. A **622**, 593 (1997).

[35] W. Cassing, L. Tolos, E. L. Bratkovskaya, and A. Ramos, Nucl. Phys. A **727**, 59 (2003).

[36] C. Fuchs, A. Faessler, E. Zabrodin, and Y.-M. Zheng, Phys. Rev. Lett. **86**, 1974 (2001).

[37] C. Fuchs, Prog. Part. Nucl. Phys. **56**, 1 (2006).

[38] A. Mishra, E. L. Bratkovskaya, J. Schaffner-Bielich, S. Schramm, and H. Stöcker, Phys. Rev. C **70**, 044904 (2004).

[39] E. E. Kolomeitsev *et al.*, J. Phys. G **31**, S741 (2005).

[40] J. Rafelski and B. Muller, Phys. Rev. Lett. **48**, 1066 (1982); **56**, 2334(E) (1986).

[41] R. Stock, J. Phys. G **28**, 1517 (2002).

[42] P. Koch, B. Muller, and J. Rafelski, Z. Phys. A **324**, 453 (1986).

[43] K. Werner and J. Aichelin, Phys. Lett. B **308**, 372 (1993).

[44] H.-J. Drescher, J. Aichelin, and K. Werner, Phys. Rev. D: Part. Fields **65**, 057501 (2002).

[45] J. Aichelin and K. Werner, Phys. Rev. C **79**, 064907 (2009); **81**, 029902(E) (2010).

[46] S. V. Afanasiev *et al.* (NA49 Collaboration), Phys. Rev. C **66**, 054902 (2002).

[47] C. Alt *et al.* (NA49 Collaboration), Phys. Rev. C **77**, 024903 (2008).

[48] B. B. Back *et al.* (E917 Collaboration), Phys. Rev. C **69**, 054901 (2004).

[49] J. Adams *et al.* (STAR Collaboration), Phys. Lett. B **612**, 181 (2005).

[50] C. Alt *et al.* (NA49 Collaboration), Phys. Rev. C **78**, 044907 (2008).

[51] M. Gazdzicki and M. I. Gorenstein, Acta Phys. Polon. B **30**, 2705 (1999).

[52] W. Cassing, A. Palmese, P. Moreau, and E. L. Bratkovskaya, Phys. Rev. C **93**, 014902 (2016).

[53] A. Palmese, W. Cassing, E. Seifert, T. Steinert, P. Moreau, and E. L. Bratkovskaya, Phys. Rev. C **94**, 044912 (2016).

[54] W. Cassing and E. L. Bratkovskaya, Phys. Rev. C **78**, 034919 (2008).

[55] W. Cassing, Eur. Phys. J. Spec. Top. **168**, 3 (2009).

[56] W. Cassing and E. L. Bratkovskaya, Nucl. Phys. A **831**, 215 (2009).

[57] E. L. Bratkovskaya, W. Cassing, V. P. Konchakovski, and O. Linnyk, Nucl. Phys. A **856**, 162 (2011).

[58] O. Linnyk, E. L. Bratkovskaya, and W. Cassing, Prog. Part. Nucl. Phys. **87**, 50 (2016).

[59] P. Moreau, O. Soloveva, L. Oliva, T. Song, W. Cassing, and E. Bratkovskaya, Phys. Rev. C **100**, 014911 (2019).

[60] J. S. Schwinger, Phys. Rev. **82**, 664 (1951).

[61] S. Okubo, Phys. Lett. **5**, 165 (1963).

[62] G. Zweig, An SU(3) model for strong interaction symmetry and its breaking, Version 2, Report No. CERN-TH-412, NP-14146, PRINT-64-170 (1964).

[63] J. Iizuka, Prog. Theor. Phys. Suppl. **37**, 21 (1966).

[64] J. Adamczewski-Musch *et al.* (HADES Collaboration), Phys. Lett. B **778**, 403 (2018).

[65] N. Herrmann (FOPI Collaboration), Nucl. Phys. A **610**, 49C (1996).

[66] K. Piasecki *et al.* (FOPI Collaboration), Phys. Rev. C **94**, 014901 (2016).

[67] M. S. Abdallah *et al.* (STAR Collaboration), Phys. Lett. B **831**, 137152 (2022).

[68] W. S. Chung, G.-Q. Li, and C. M. Ko, Nucl. Phys. A **625**, 347 (1997).

[69] H. Schade, G. Wolf, and B. Kampfer, Phys. Rev. C **81**, 034902 (2010).

[70] J. Steinheimer and M. Bleicher, J. Phys. G **43**, 015104 (2016).

[71] Y. Maeda *et al.* (ANKE Collaboration), Phys. Rev. C **77**, 015204 (2008).

[72] V. Steinberg, J. Staudenmaier, D. Oliinychenko, F. Li, O. Erkiner, and H. Elfner, Phys. Rev. C **99**, 064908 (2019).

[73] L. Fabbietti (HADES Collaboration), AIP Conf. Proc. **1701**, 040005 (2016).

[74] P. A. Zyla *et al.* (Particle Data Group), PTEP **2020**, 083C01 (2020).

[75] T. Song, L. Tolos, J. Wirth, J. Aichelin, and E. Bratkovskaya, Phys. Rev. C **103**, 044901 (2021).

[76] G. E. Brown and M. Rho, Phys. Rev. Lett. **66**, 2720 (1991).

[77] T. Hatsuda and S. H. Lee, Phys. Rev. C **46**, R34 (1992).

[78] F. Klingl, T. Waas, and W. Weise, Phys. Lett. B **431**, 254 (1998).

[79] E. Oset and A. Ramos, Nucl. Phys. A **679**, 616 (2001).

[80] D. Cabrera and M. J. Vicente Vacas, Phys. Rev. C **67**, 045203 (2003).

[81] P. Gubler and W. Weise, Nucl. Phys. A **954**, 125 (2016).

[82] J. Kim, P. Gubler, and S. H. Lee, arXiv:2204.11440.

[83] R. Muto *et al.* (KEK-PS-E325 Collaboration), Phys. Rev. Lett. **98**, 042501 (2007).

[84] H. Sako *et al.*, Proposal for the 32nd J-PARC PAC Meeting (2022).

[85] A. Ilner, J. Blair, D. Cabrera, C. Markert, and E. Bratkovskaya, Phys. Rev. C **99**, 024914 (2019).

[86] D. Gamermann, C. Garcia-Recio, J. Nieves, and L. L. Salcedo, Phys. Rev. D **84**, 056017 (2011).

[87] W. Cassing, E. S. Golubeva, A. S. Ilinov, and L. A. Kondratyuk, Phys. Lett. B **396**, 26 (1997).

[88] E. L. Bratkovskaya and C. M. Ko, Phys. Lett. B **445**, 265 (1999).

[89] E. L. Bratkovskaya, Phys. Lett. B **529**, 26 (2002).

[90] E. L. Bratkovskaya and W. Cassing, Nucl. Phys. A **807**, 214 (2008).

[91] O. Kaymakcalan, S. Rajeev, and J. Schechter, Phys. Rev. D: Part. Fields **30**, 594 (1984).

[92] D. Cabrera, A. N. Hiller Blin, and M. J. Vicente Vacas, Phys. Rev. C **95**, 015201 (2017).

[93] D. Trnka *et al.* (CBELSA/TAPS Collaboration), Phys. Rev. Lett. **94**, 192303 (2005).

[94] V. Metag, Prog. Part. Nucl. Phys. **61**, 245 (2008).

[95] W. Cassing and S. Juchem, Nucl. Phys. A **665**, 377 (2000).

[96] W. Cassing and S. Juchem, Nucl. Phys. A **672**, 417 (2000).

[97] L. P. Kadanoff and G. Baym, *Quantum Statistical Mechanics* (W. A. Benjamin, Inc., New York, 1962).

[98] S. Juchem, W. Cassing, and C. Greiner, Nucl. Phys. A **743**, 92 (2004).

[99] W. Cassing, Nucl. Phys. A **700**, 618 (2002).

[100] E. Seifert and W. Cassing, Phys. Rev. C **97**, 024913 (2018).

[101] W. Cassing, Lect. Notes Phys. **989** (2021).

[102] A. Baldini, V. Flaminio, W. G. Moorhead, and D. R. O. Morrison, *Total Cross-Sections for Reactions of High Energy Particles (Including Elastic, Topological, Inclusive and Exclusive Reactions), Totale Wirkungsquerschnitte für Reaktionen hochenergetischer Teilchen (einschließlich elastischer, topologischer, inklusive*, Vol. 12b of *Landolt-Boernstein - Group I Elementary Particles, Nuclei and Atoms* (Springer, Berlin, Heidelberg, 1988).

[103] F. Balestra *et al.* (DISTO Collaboration), Phys. Rev. C **63**, 024004 (2001).

[104] F. Balestra *et al.* (DISTO Collaboration), Phys. Rev. Lett. **89**, 092001 (2002).

[105] P. Moskal, M. Wolke, A. Khoukaz, and W. Oelert, Prog. Part. Nucl. Phys. **49**, 1 (2002).

[106] D. Drijard *et al.* (Annecy(LAPP)-CERN-College de France-Dortmund-Heidelberg-Warsaw Collaboration), Z. Phys. C: Part. Fields **9**, 293 (1981).

[107] C. Daum *et al.* (ACCMOR Collaboration), Nucl. Phys. B **186**, 205 (1981).

[108] Y. M. Antipov *et al.*, Phys. Lett. B **110**, 326 (1982).

[109] V. Blobel, H. Fesefeldt, H. Franz, A. Hofmann, C. Jetter, H. Neumann, B. Schroder, and P. Soding, Phys. Lett. B **59**, 88 (1975).

[110] F. Balestra *et al.* (DISTO Collaboration), Phys. Lett. B **468**, 7 (1999).

[111] S. V. Afanasiev *et al.* (NA49 Collaboration), Phys. Lett. B **491**, 59 (2000).

[112] R. Rapp and J. Wambach, Adv. Nucl. Phys. **25**, 1 (2000).

[113] D. Cabrera, L. Tolós, J. Aichelin, and E. Bratkovskaya, Phys. Rev. C **90**, 055207 (2014).

[114] E. L. Bratkovskaya and W. Cassing, Nucl. Phys. A **619**, 413 (1997).

[115] A. Sibirtsev and W. Cassing, Nucl. Phys. A **641**, 476 (1998).

[116] B. Nilsson-Almqvist and E. Stenlund, Comput. Phys. Commun. **43**, 387 (1987).

[117] V. Kireyeu, I. Grishmanovskii, V. Kolesnikov, V. Voronyuk, and E. Bratkovskaya, Eur. Phys. J. A **56**, 223 (2020).

[118] Y. S. Golubeva, L. A. Kondratyuk, and W. Cassing, Nucl. Phys. A **625**, 832 (1997).

[119] S. Pal, C. M. Ko, and Z.-w. Lin, Nucl. Phys. A **707**, 525 (2002).

[120] Z.-W. Lin, C. M. Ko, B.-A. Li, B. Zhang, and S. Pal, Phys. Rev. C **72**, 064901 (2005).

[121] C. M. Ko and B. H. Sa, Phys. Lett. B **258**, 6 (1991).

[122] E. Oset and A. Ramos, Nucl. Phys. A **635**, 99 (1998).

[123] J. Nieves and E. Ruiz Arriola, Phys. Rev. D: Part. Fields **64**, 116008 (2001).

[124] S. Spies (HADES Collaboration), *29th International Conference on Ultra-relativistic Nucleus-Nucleus Collisions* (2022).

[125] A. Forster *et al.*, Phys. Rev. C **75**, 024906 (2007).

[126] H. Schuldes (HADES Collaboration), Nucl. Phys. A **967**, 804 (2017).

[127] S. Spies (HADES Collaboration), EPJ Web Conf. **259**, 01007 (2022).

[128] L. Ahle *et al.* (E866 and E917 Collaborations), Phys. Lett. B **490**, 53 (2000).

[129] F. Li, L.-W. Chen, C. M. Ko, and S. H. Lee, Phys. Rev. C **85**, 064902 (2012).

[130] L.-W. Chen, C. M. Ko, and Y. Tzeng, Phys. Lett. B **584**, 269 (2004).

[131] C. H. Li and C. M. Ko, Nucl. Phys. A **712**, 110 (2002).

[132] K. Piasecki *et al.* (FOPI Collaboration), Phys. Rev. C **99**, 014904 (2019).